Electronic Supplementary Material (ESI) for New Journal of Chemistry.

Electronic Supplementary Information

Multifunctionality of the $[C_2mim][Ln(fod)_4]$ series (Ln = Nd-Tm except Pm): Magnetic, Luminescent and Thermochemical studies

Ana C. Cerdeira [1], João P. Leal [2], João Avó [3], Catarina Viola [4], Maria H. Casimiro [5], Luis M. Ferreira [1], Filipe A. A. Paz [6], Laura C. J. Pereira [1,*], Cláudia C. L. Pereira [4,*] and Bernardo Monteiro [7,*]

[1] Centro de Ciências e Tecnologias Nucleares (C2TN), DECN, Instituto Superior Técnico, Universidade de Lisboa, Campus Tecnológico e Nuclear, Estrada Nacional 10, 2695-066 Bobadela, Portugal.

[2] Centro de Química Estrutural (CQE), Institute of Molecular Sciences, DECN, Instituto Superior Técnico, Universidade de Lisboa, Campus Tecnológico e Nuclear, Estrada Nacional 10, 2695-066 Bobadela, Portugal.

[3] Associate Laboratory i4HB—Institute for Health and Bioeconomy and Institute for Bioengineering and Biosciences (IBB), Instituto Superior Técnico, Universidade de Lisboa, Av. Rovisco Pais, 1049-001 Lisboa, Portugal.

[4] LAQV-REQUIMTE, Dep. de Química, Universidade Nova de Lisboa,2829-516, Monte de Caparica, Portugal.

[5] Centro de Ciências e Tecnologias Nucleares (C2TN), Instituto Superior Técnico, Universidade de Lisboa, Campus Tecnológico e Nuclear, Estrada Nacional 10, 2695-066 Bobadela, Portugal.

[6] Department of Chemistry, CICECO-Aveiro Institute of Materials, University of Aveiro, 3810-193 Aveiro, Portugal.

[7] Centro de Química Estrutural (CQE), Institute of Molecular Sciences, DEQ, Instituto Superior Técnico, Universidade de Lisboa, Campus Tecnológico e Nuclear, Estrada Nacional 10, 2695-066 Bobadela, Portugal.

* Correspondence: lpereira@ctn.tecnico.ulisboa.pt (LCJP); ccl.pereira@fct.unl.pt (CCLP); bernardo.monteiro@ctn.tecnico.ulisboa.pt (BM).

Contents:

1) ESI-MS

ESI-MS analysis of compounds [C_2mim][Eu(fod)$_4$] and [C_2mim][Tb(fod)$_4$] were presented in ref. 10 and 29 of the main manuscript, respectively. Additionally, we made more 5 for control.

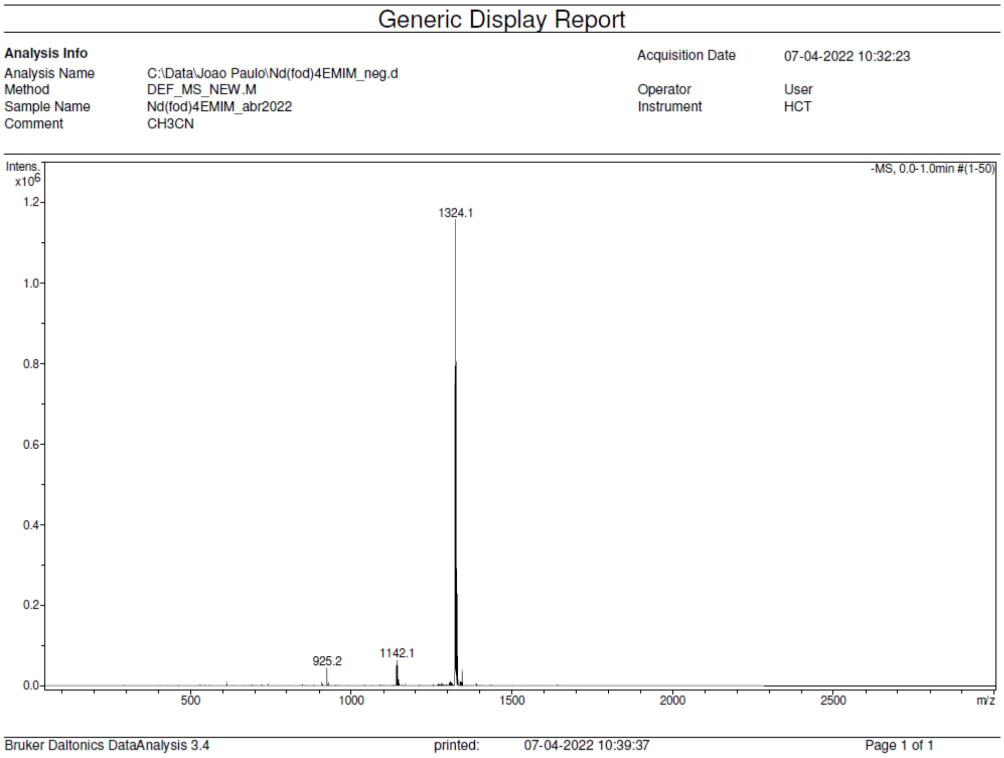

Figure S1. ESI-MS analysis of [C_2mim][Nd(fod)$_4$] in acetonitrile, negative mode.

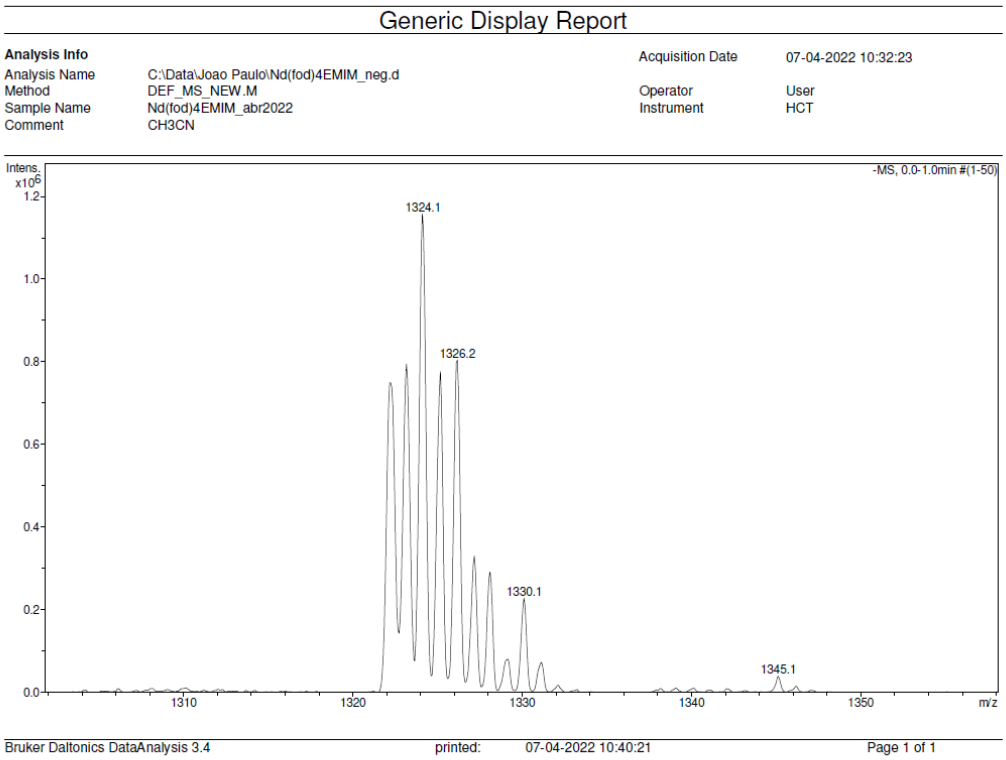

Figure S2. Expanded ESI-MS analysis of [C_2mim][Nd(fod)$_4$] in acetonitrile, negative mode.

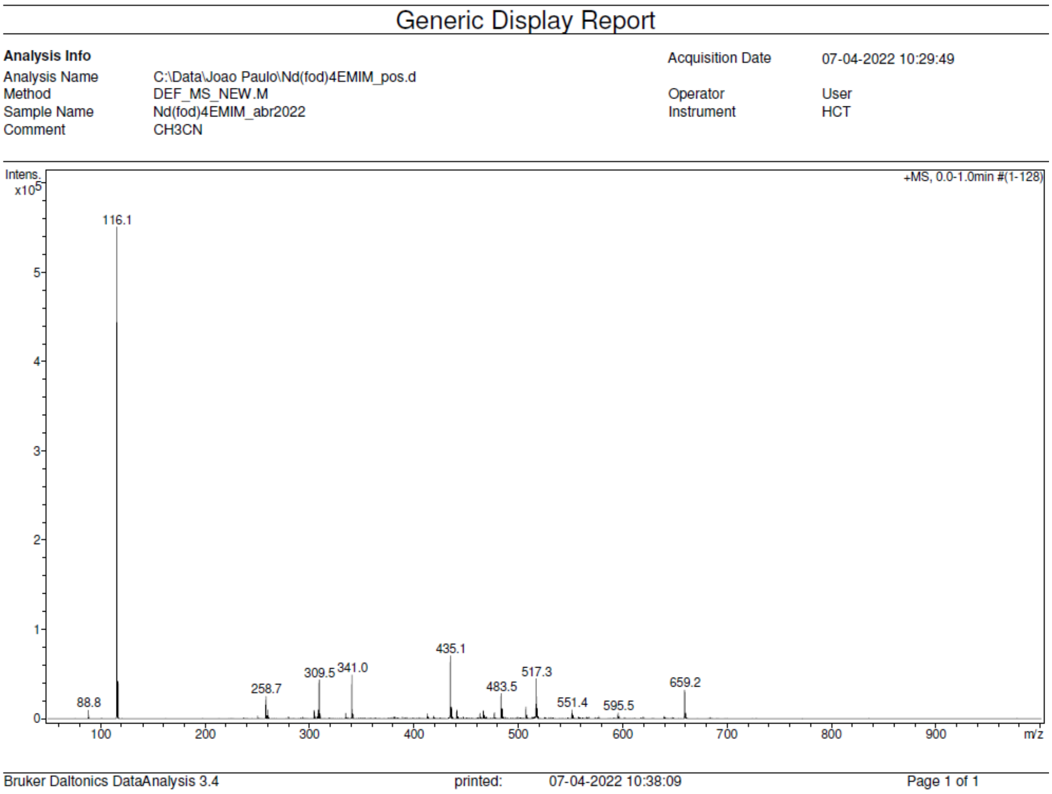

Figure S3. ESI-MS analysis of $[C_2mim][Nd(fod)_4]$ in acetonitrile, positive mode.

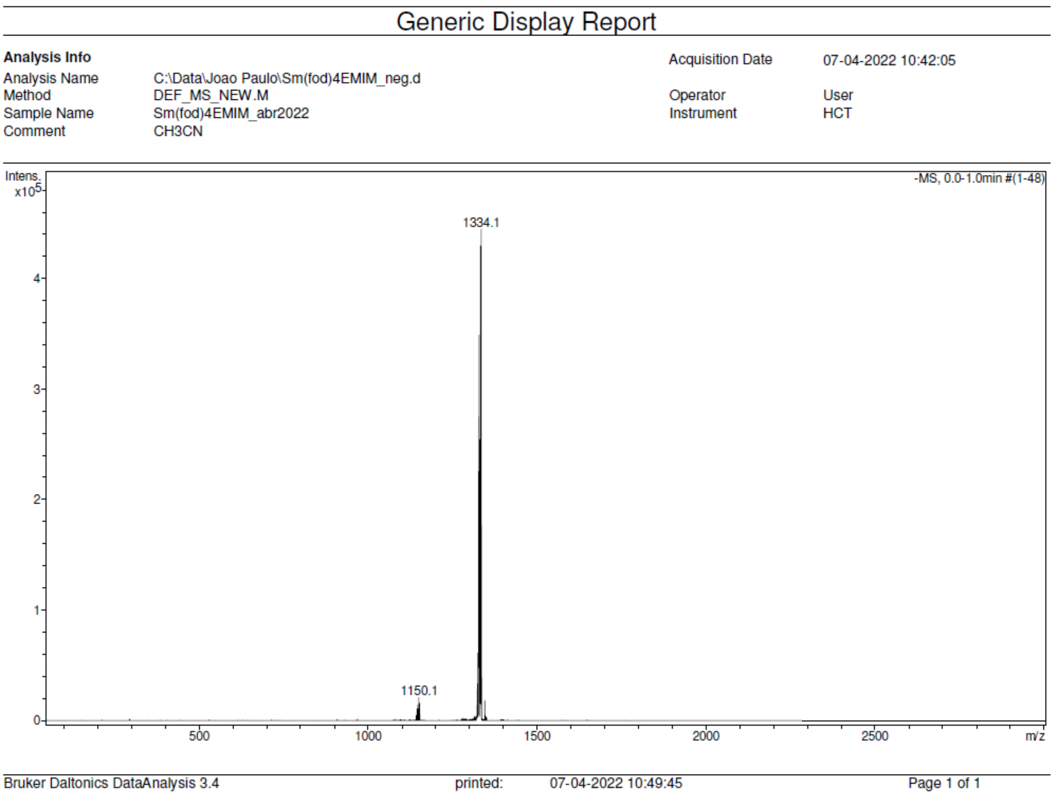

Figure S4. ESI-MS analysis of $[C_2mim][Sm(fod)_4]$ in acetonitrile, negative mode.

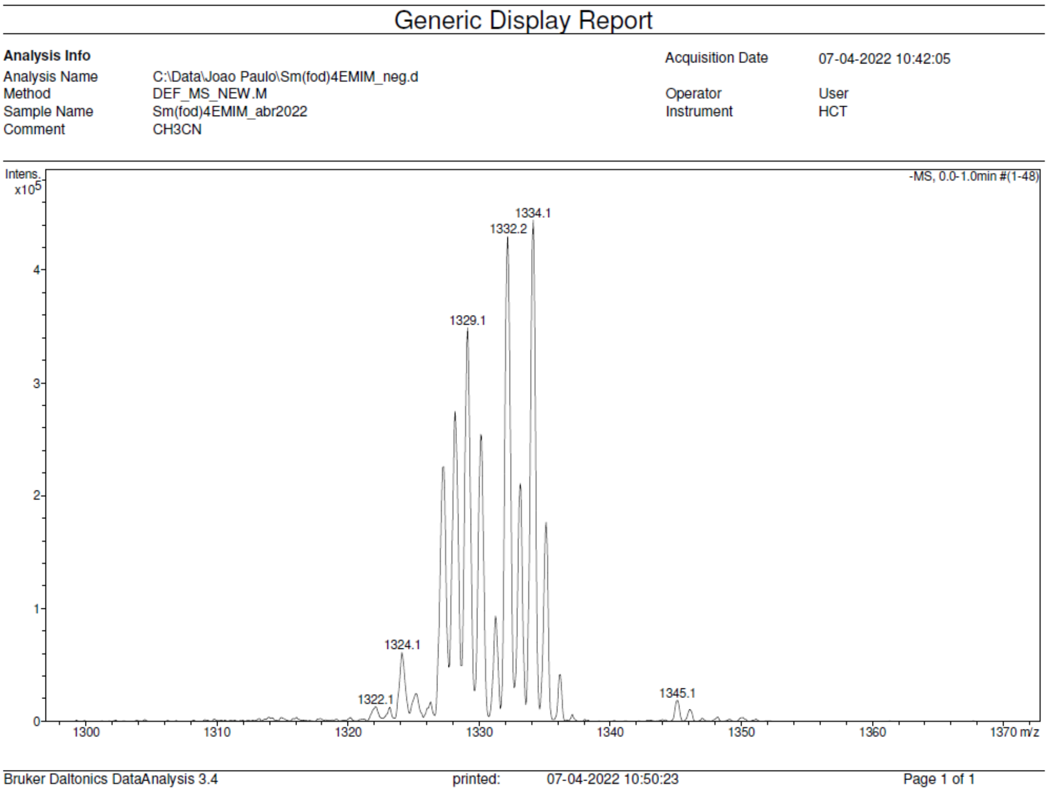

Figure S5. Expanded ESI-MS analysis of $[C_2mim][Sm(fod)_4]$ in acetonitrile, negative mode.

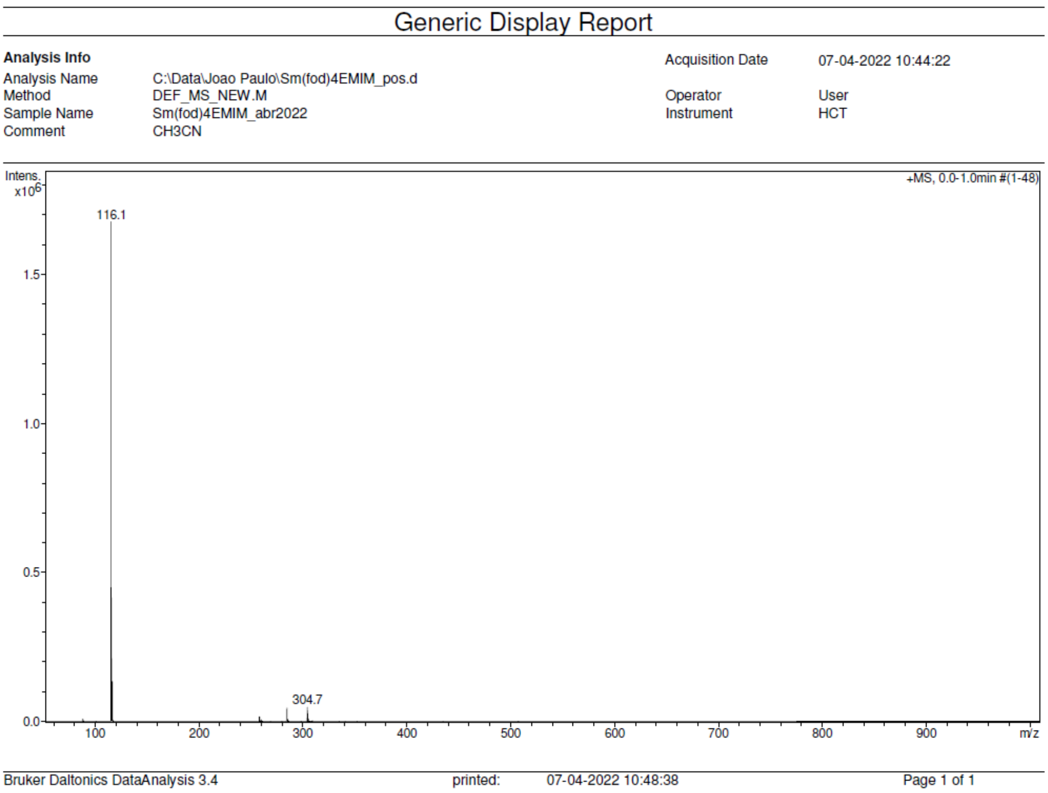

Figure S6. ESI-MS analysis of $[C_2mim][Sm(fod)_4]$ in acetonitrile, positive mode.

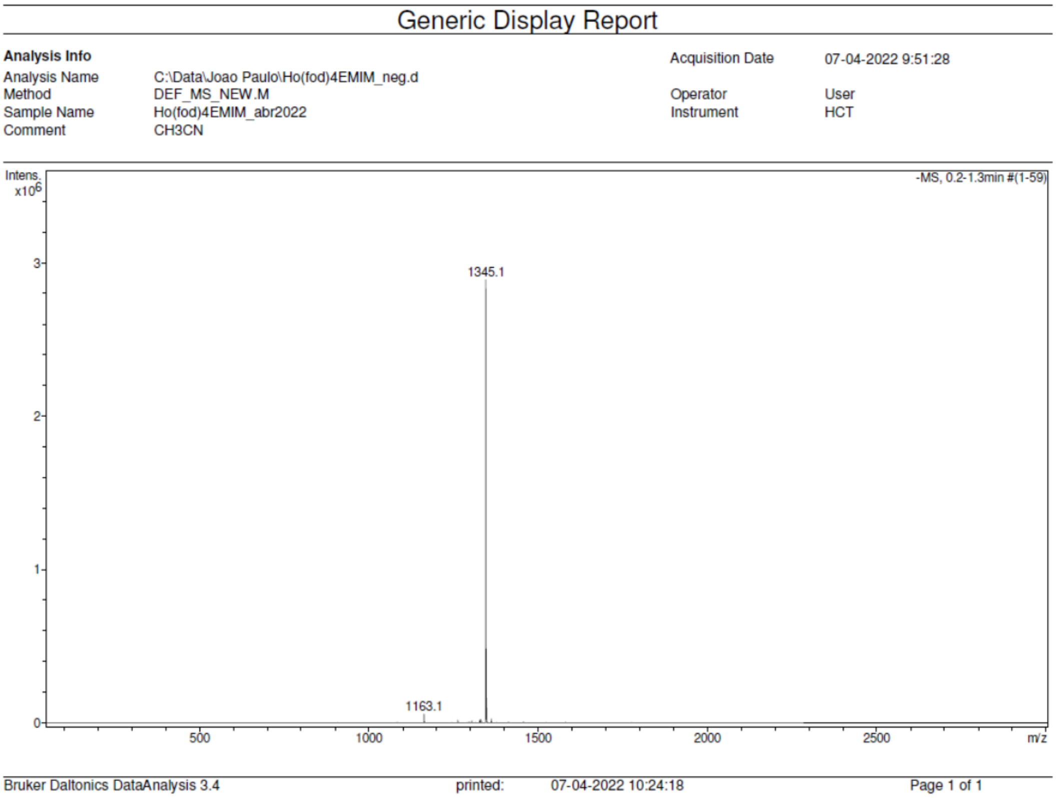

Figure S7. Expanded ESI-MS analysis of $[C_2mim][Ho(fod)_4]$ in acetonitrile, negative mode.

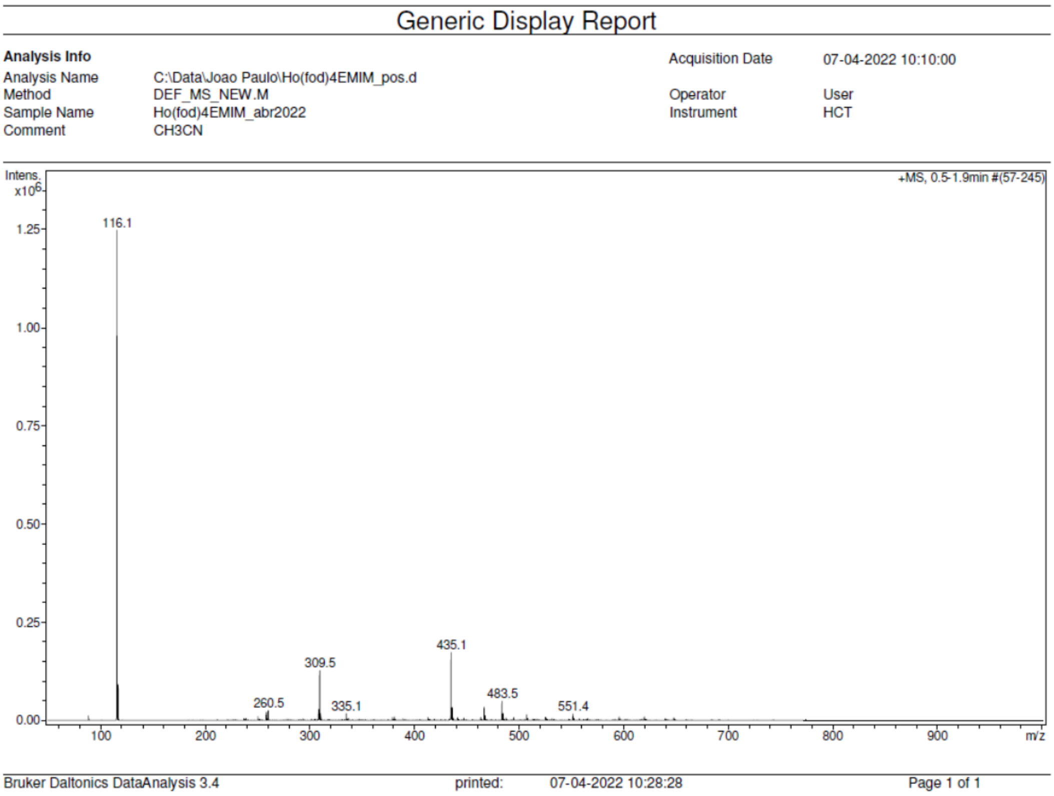

Figure S8. Expanded ESI-MS analysis of $[C_2mim][Ho(fod)_4]$ in acetonitrile, positive mode.

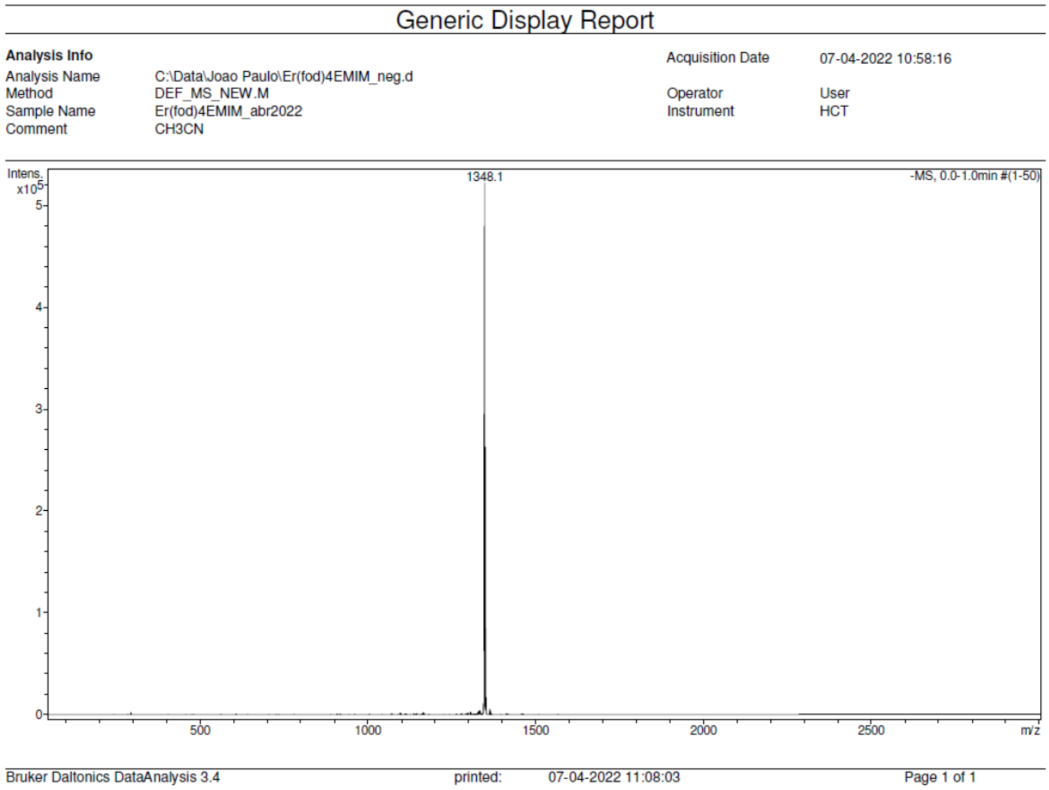

Figure S9. ESI-MS analysis of $[C_2mim][Er(fod)_4]$ in acetonitrile, negative mode.

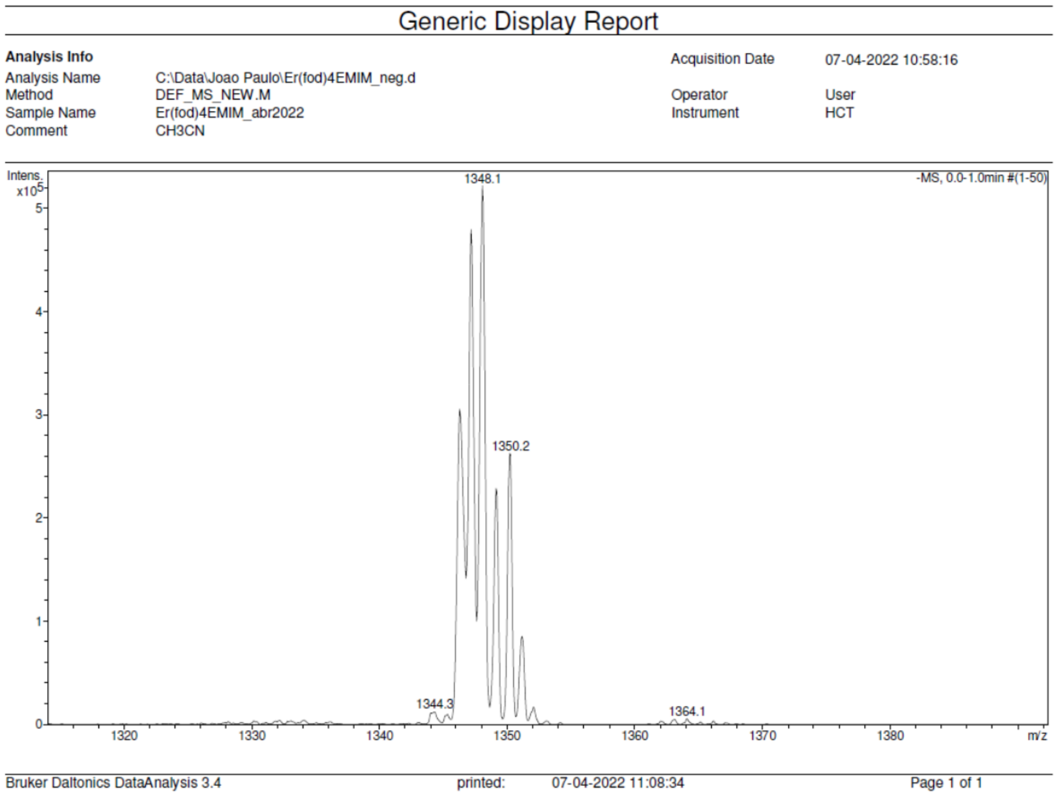

Figure S10. Expanded ESI-MS analysis of $[C_2mim][Er(fod)_4]$ in acetonitrile, negative mode.

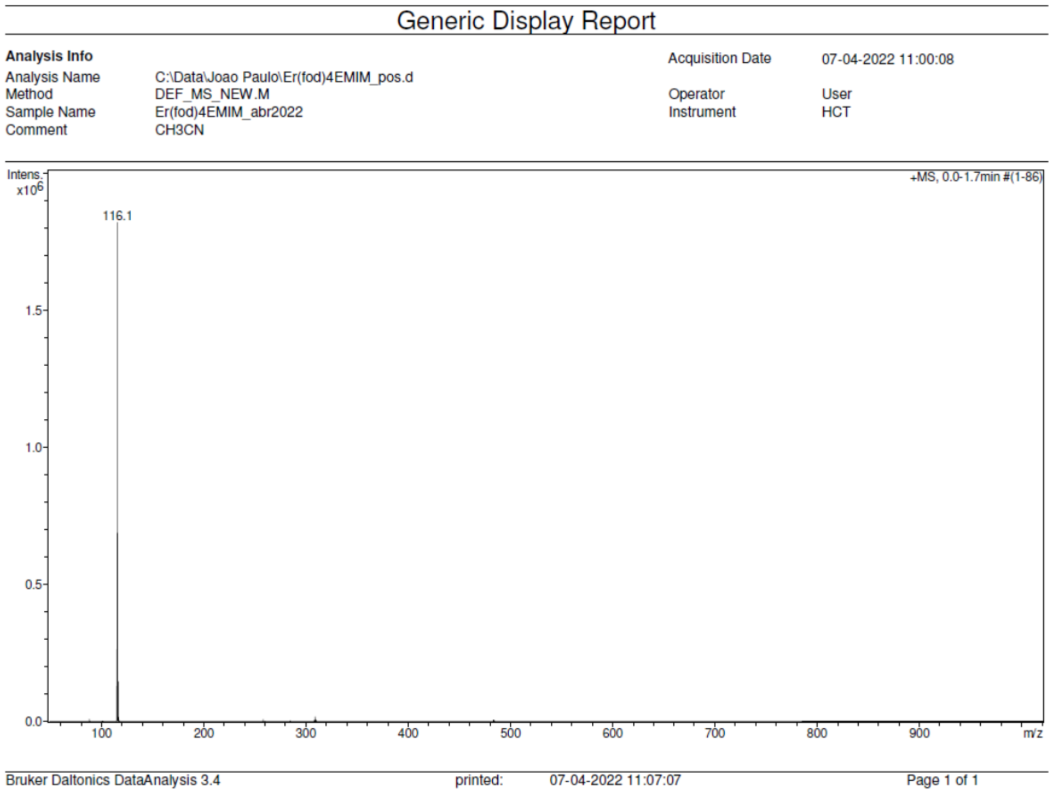

Figure S11. ESI-MS analysis of $[C_2mim][Er(fod)_4]$ in acetonitrile, positive mode.

1) FT-IR

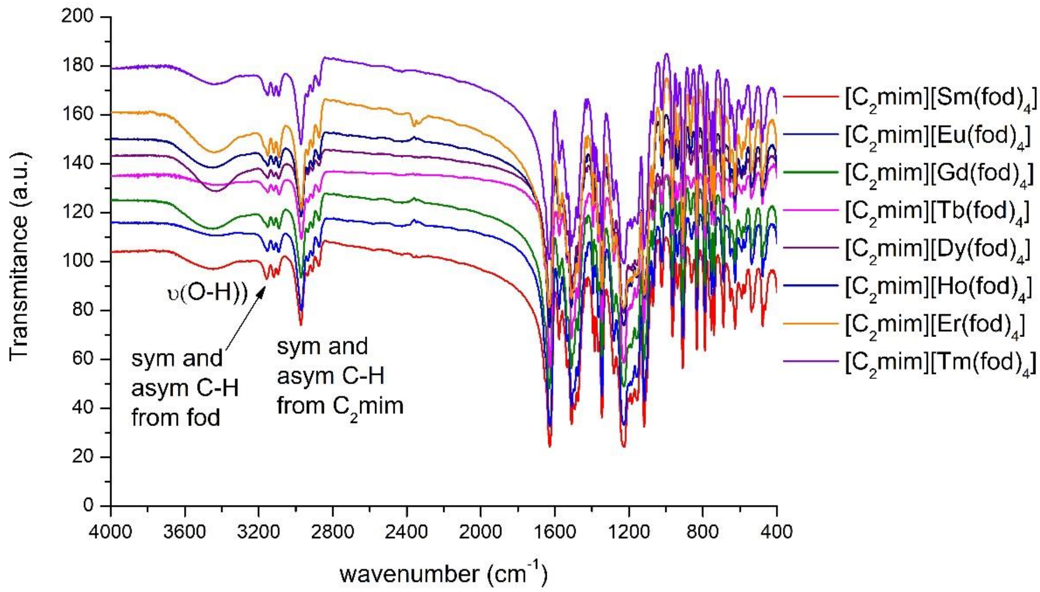

Figure S12. FT-IR spectra for compounds **2-9** in the 400 - 4000 cm^{-1} range.

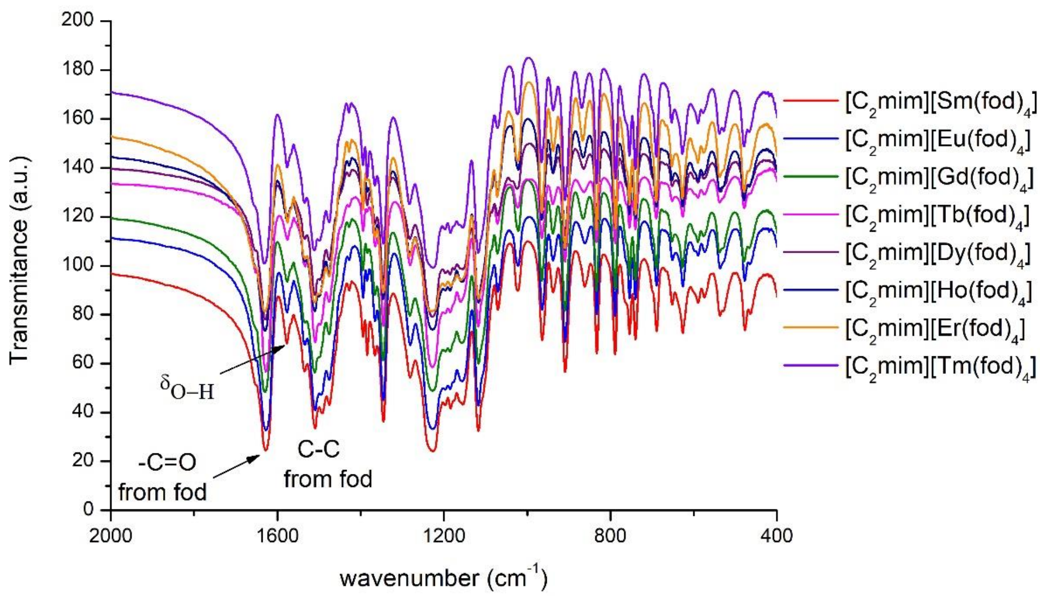

Figure S13. FT-IR spectra for compounds **2-9** in the 400 - 2000 cm^{-1} range.

2) Powder X-ray diffraction studies

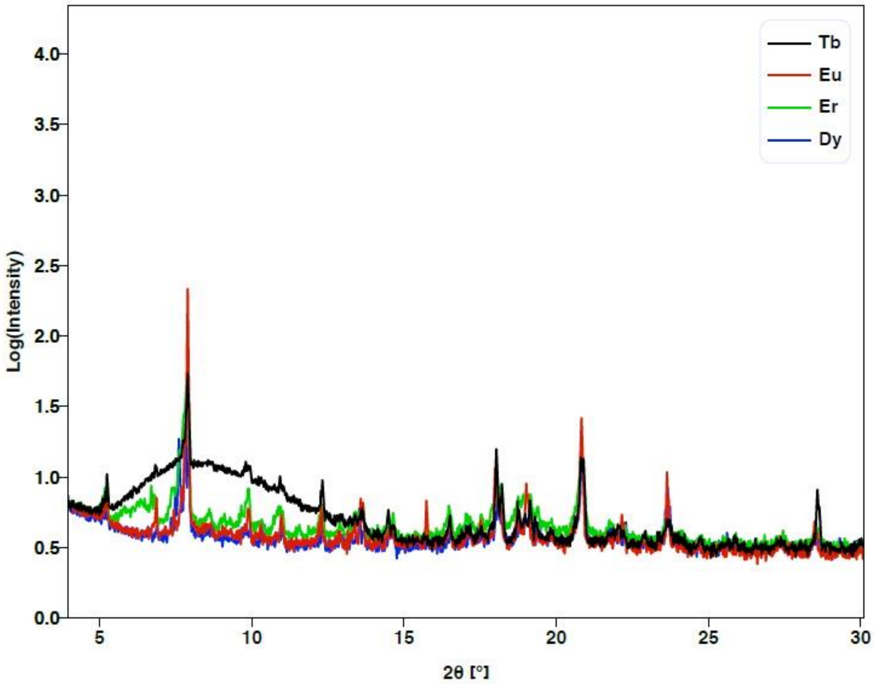

Figure S14. Powder X-ray diffraction patterns made with crystals of the Eu (**3**), Tb (**5**), Dy (**6**) and Er (**8**) compounds.

3) Thermogravimetry

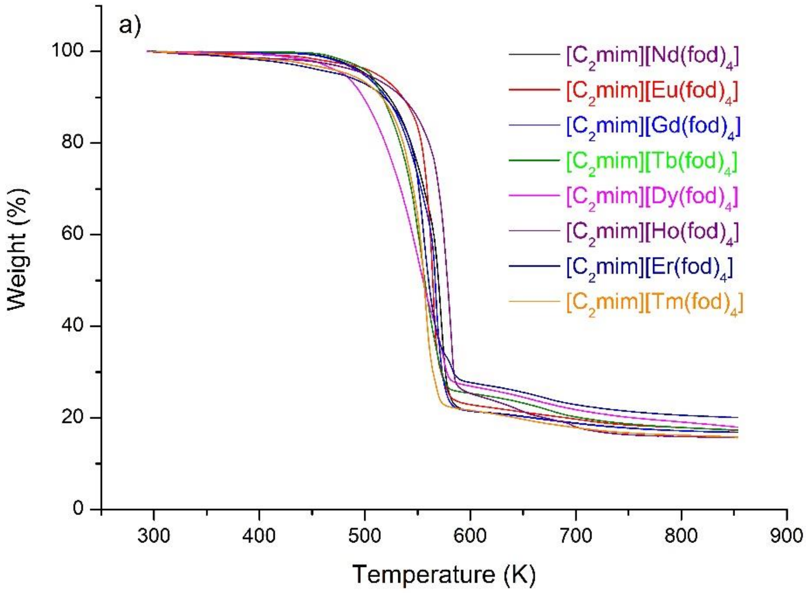

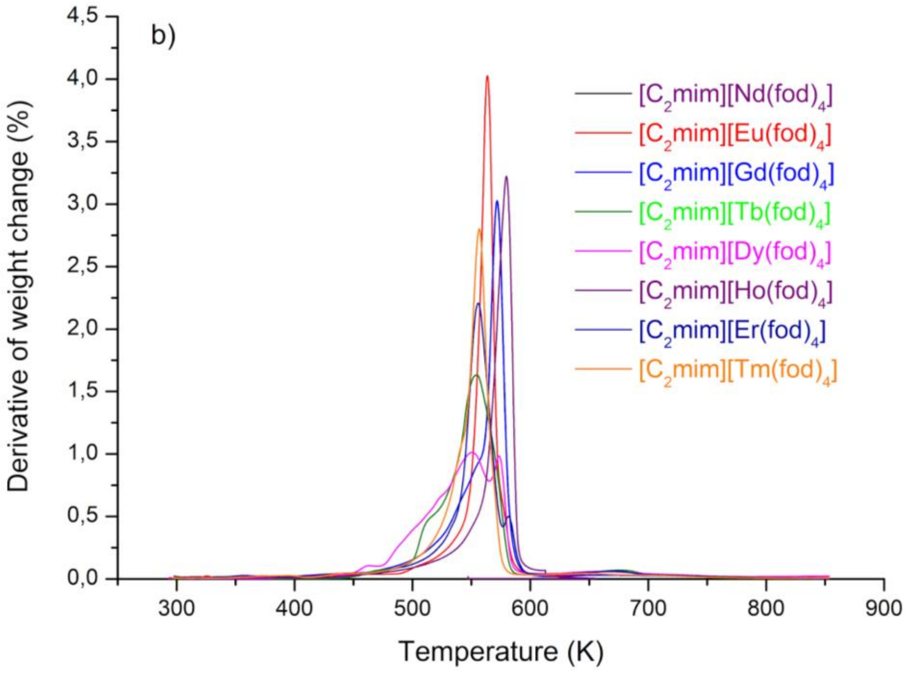

Figure S15. (a) Thermogravimetric analysis for compounds **1,3-9** between 293 and 858 K and (b) the derivative of the weight change of the Thermogravimetric results.

4) Differential scanning calorimetry Studies

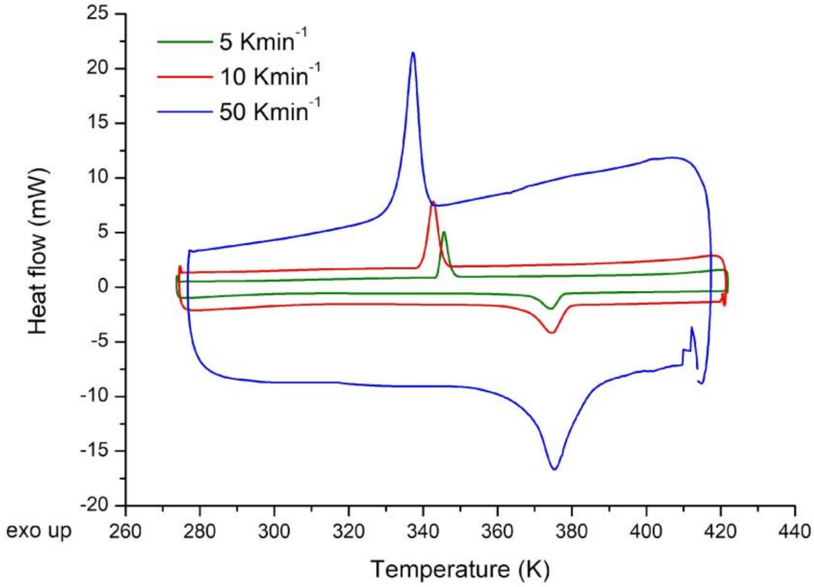

Figure S16. DSC analysis for the $[C_2mim][Nd(fod)_4]$ (**1**) compound in the range 273-423 K with a scanning rate of 5 $Kmin^{-1}$ (green), 10 $Kmin^{-1}$ (red) and 50 $Kmin^{-1}$ (blue).

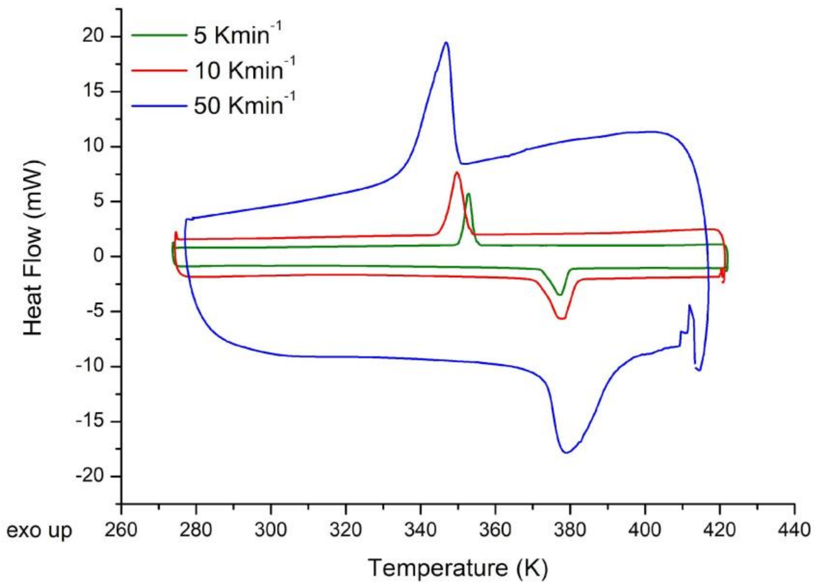

Figure S17. DSC analysis for the $[C_2mim][Sm(fod)_4]$ (**2**) compound in the range 273-423 K with a scanning rate of 5 $Kmin^{-1}$ (green), 10 $Kmin^{-1}$ (red) and 50 $Kmin^{-1}$ (blue).

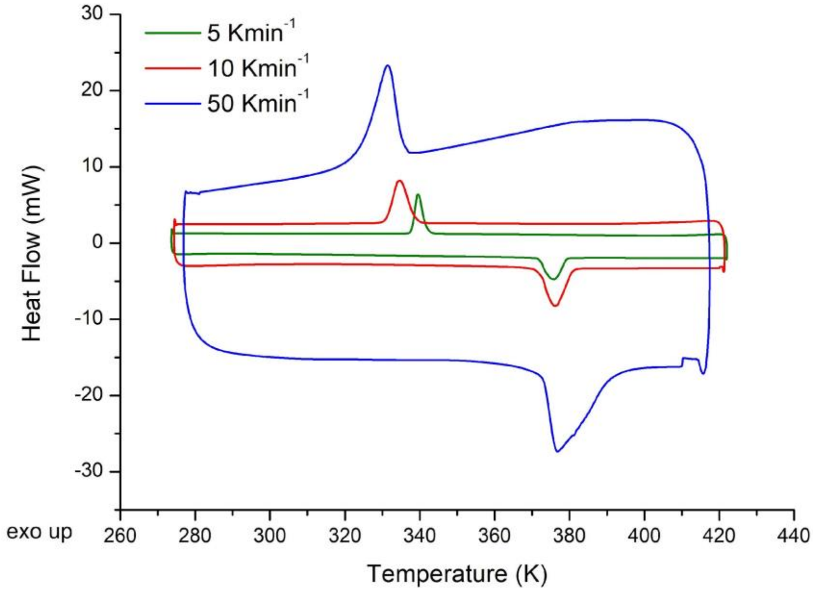

Figure S18. DSC analysis for the $[C_2mim][Eu(fod)_4]$ (**3**) compound in the range 273-423 K with a scanning rate of 5 $Kmin^{-1}$ (green), 10 $Kmin^{-1}$ (red) and 50 $Kmin^{-1}$ (blue).

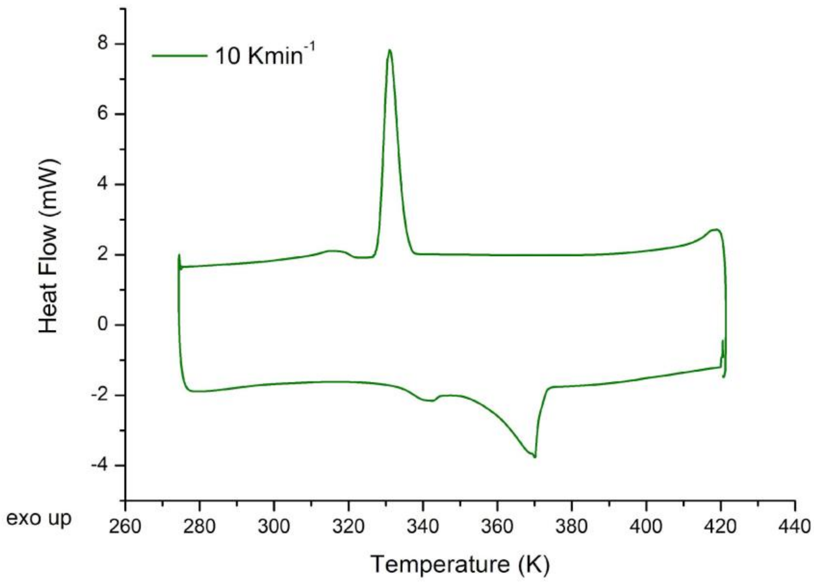

Figure S19. DSC analysis for the $[C_2mim][Gd(fod)_4]$ (**4**) compound in the range 273-423 K with a scanning rate of 10 $Kmin^{-1}$.

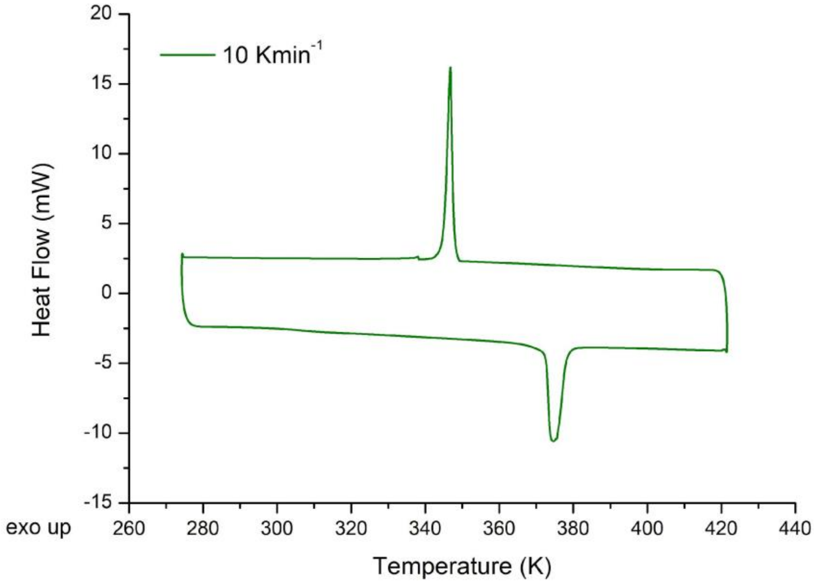

Figure S20. DSC analysis for the [C_2mim][Tb(fod)$_4$] (**5**) compound in the range 273-423 K with a scanning rate of 10 Kmin^{-1}.

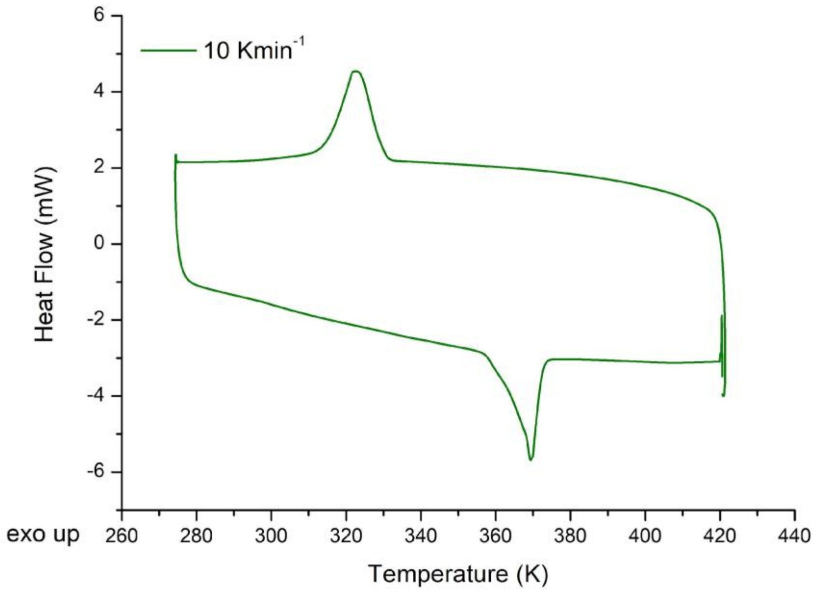

Figure S21. DSC analysis for the [C_2mim][Ho(fod)$_4$] (**7**) compound in the range 273-423 K with a scanning rate of 10 Kmin^{-1}.

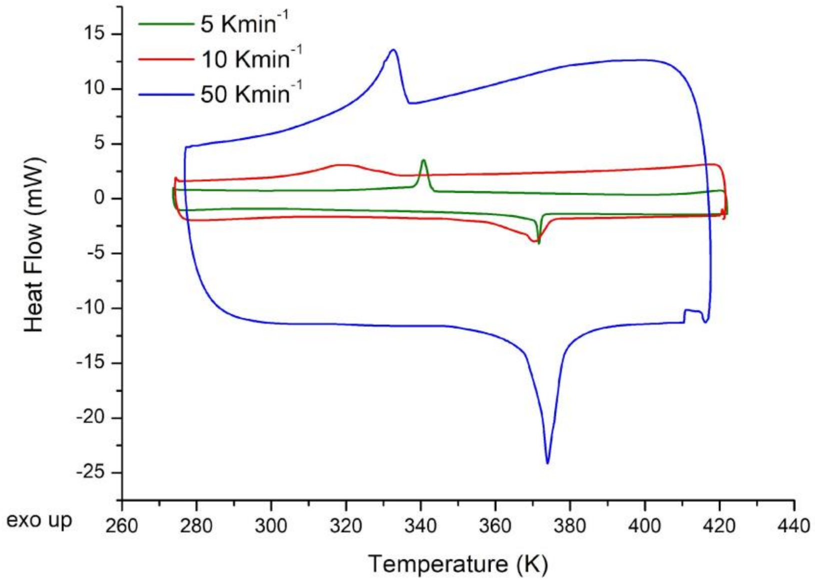

Figure S22. DSC analysis for the [C_2mim][Er(fod)$_4$] (**8**) compound in the range 273-423 K with a scanning rate of 5 Kmin^{-1} (green), 10 Kmin^{-1} (red) and 50 Kmin^{-1} (blue).

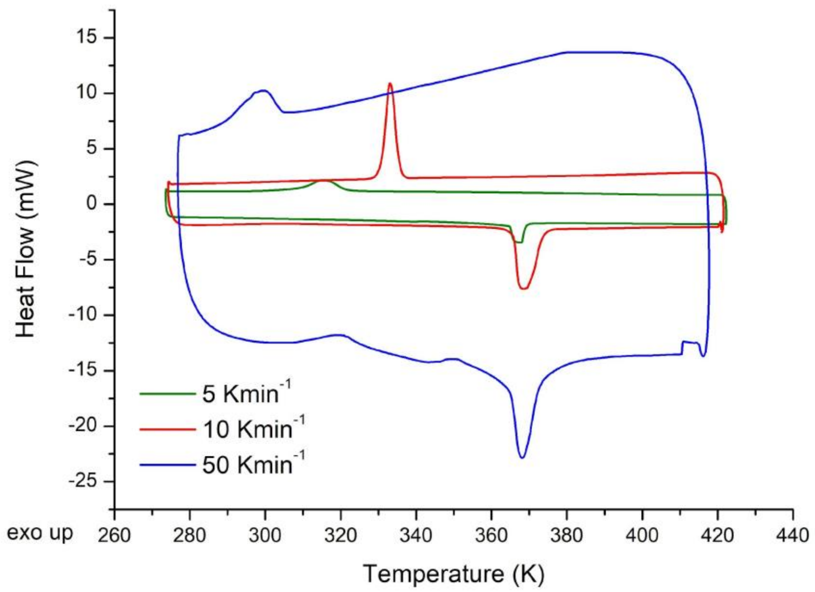

Figure S23. DSC analysis for the [C_2mim][Tm(fod)$_4$] (**9**) compound in the range 273-423 K with a scanning rate of 5 Kmin^{-1} (green), 10 Kmin^{-1} (red) and 50 Kmin^{-1} (blue).

5) Excitation spectra

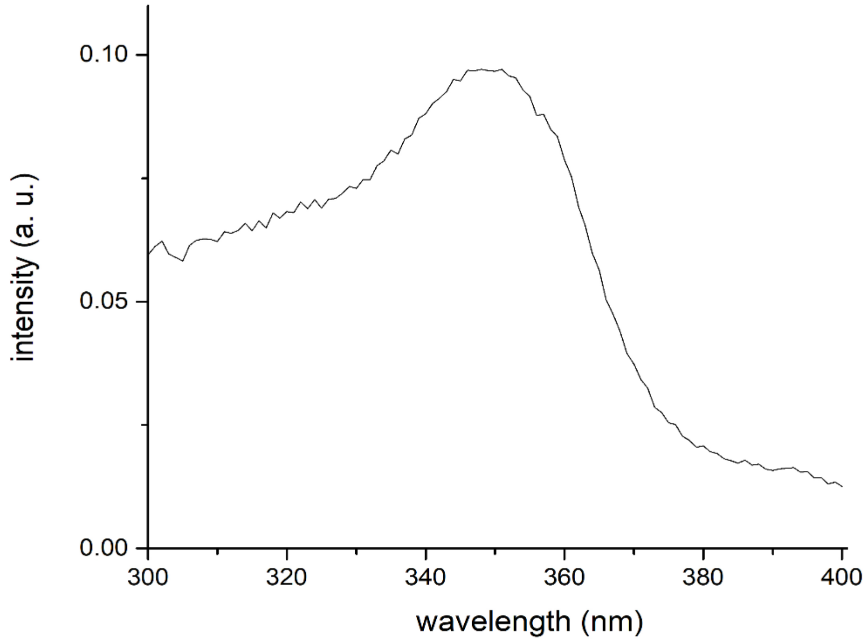

Figure S24. Excitation spectrum of the $[C_2mim][Nd(fod)_4]$ (**1**) compound.

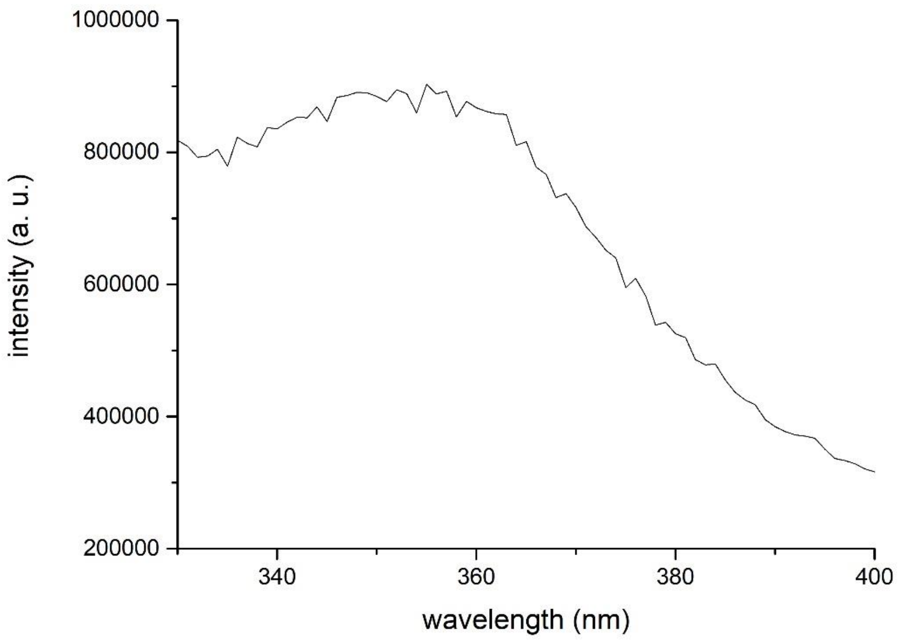

Figure S25. Excitation spectrum of the $[C_2mim][Eu(fod)_4]$ (**3**) compound.

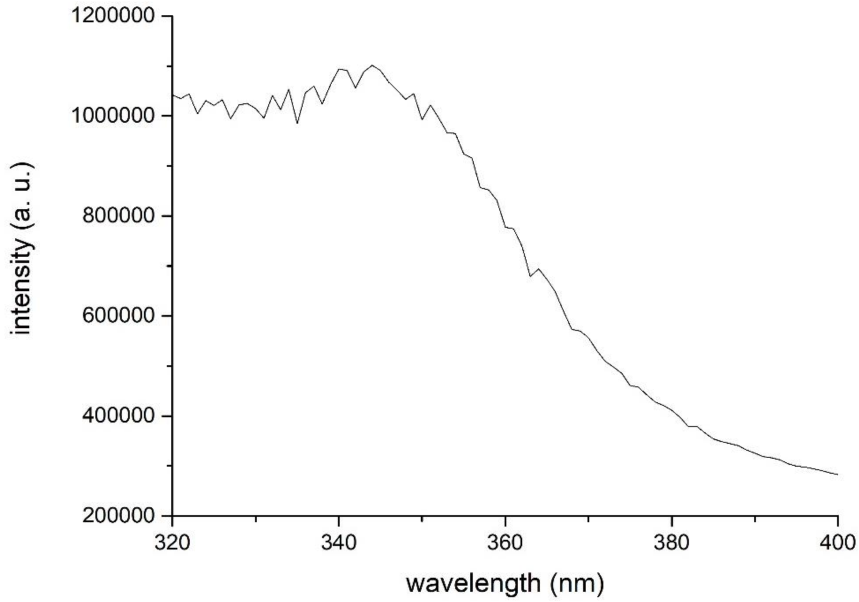

Figure S26. Excitation spectrum of the [C_2mim][Tb(fod)$_4$] (**5**) compound.

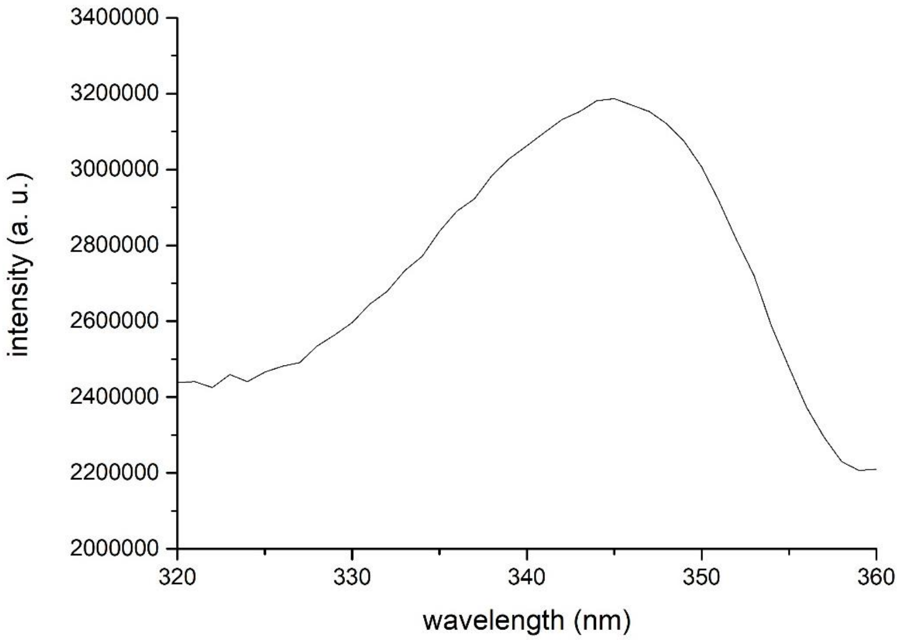

Figure S27. Excitation spectrum of the [C_2mim][Dy(fod)$_4$] (**6**) compound.

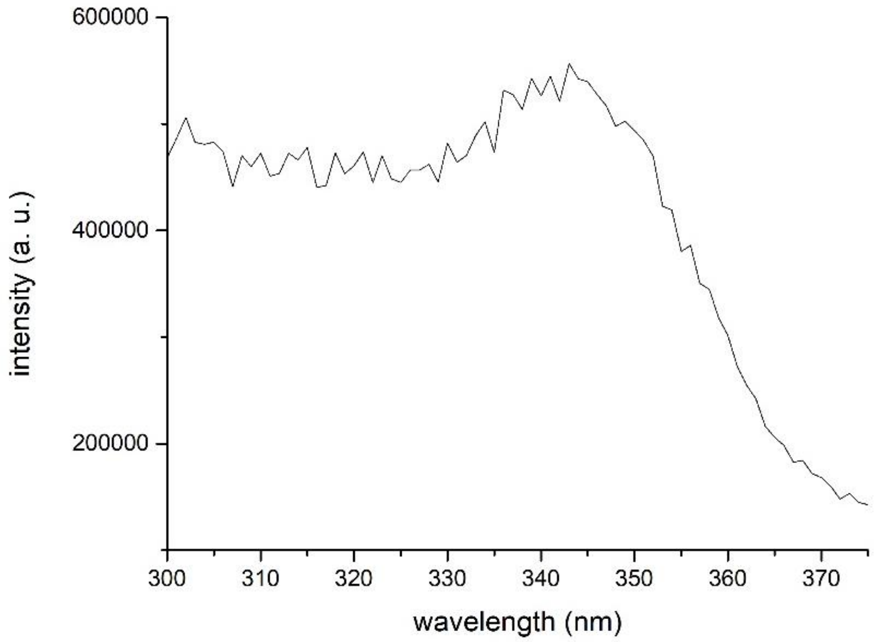

Figure S28. Excitation spectrum of the [C_2mim][Tm(fod)$_4$] (**9**) compound.

6) DC Measurements

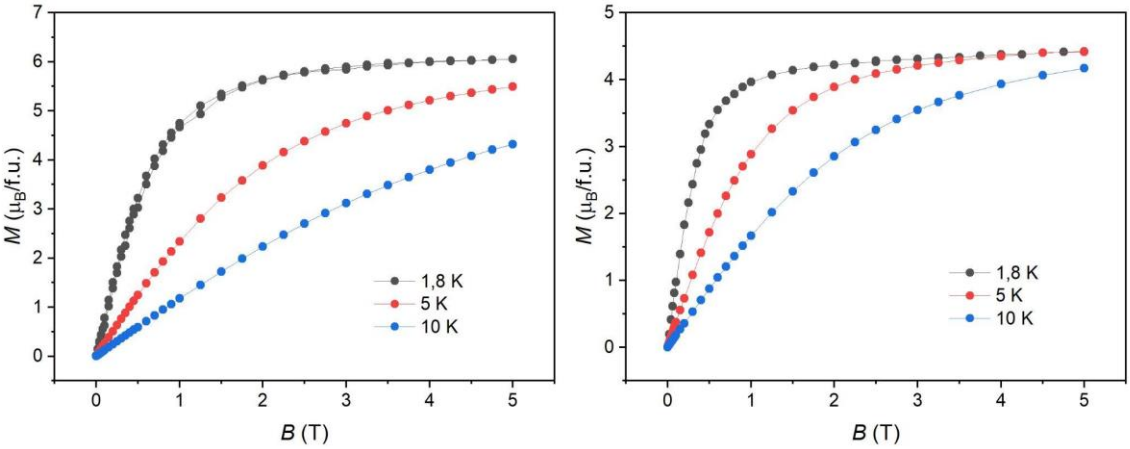

Figure S29. Field dependence of the magnetization at several temperatures for (left) [C_2mim][Gd(fod)$_4$] (**4**) and (right) [C_2mim][Tb(fod)$_4$] (**5**).

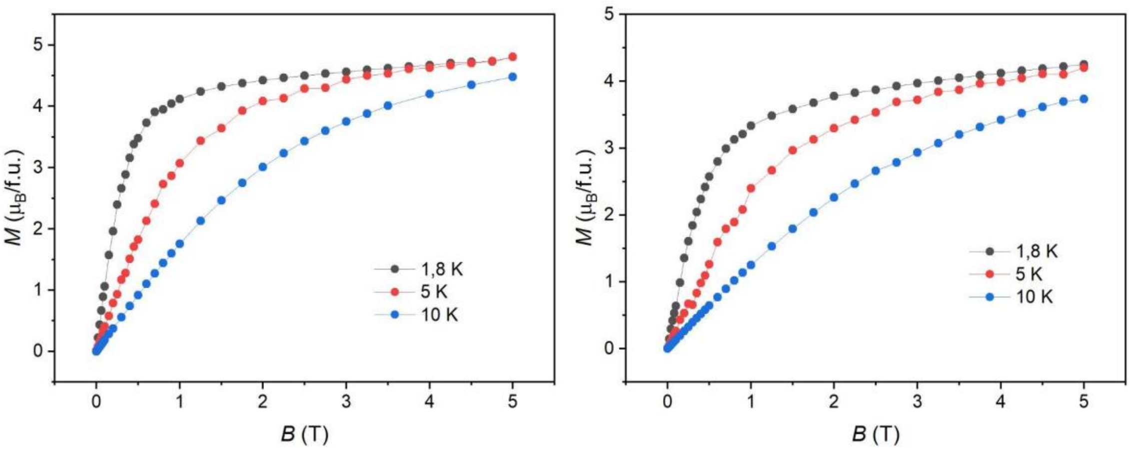

Figure S30. Field dependence of the magnetization at several temperatures for (left) [C_2mim][Dy(fod)$_4$] (**6**) and (right) [C_2mim][Ho(fod)$_4$] (**7**).

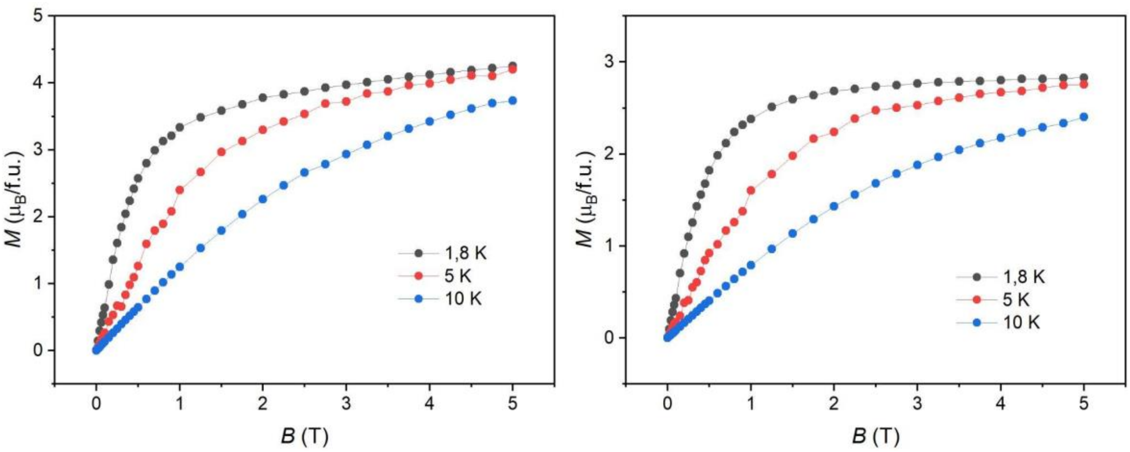

Figure S31. Field dependence of the magnetization at several temperatures for (left) [C_2mim][Er(fod)$_4$] (**8**) and (right) [C_2mim][Tm(fod)$_4$] (**9**).

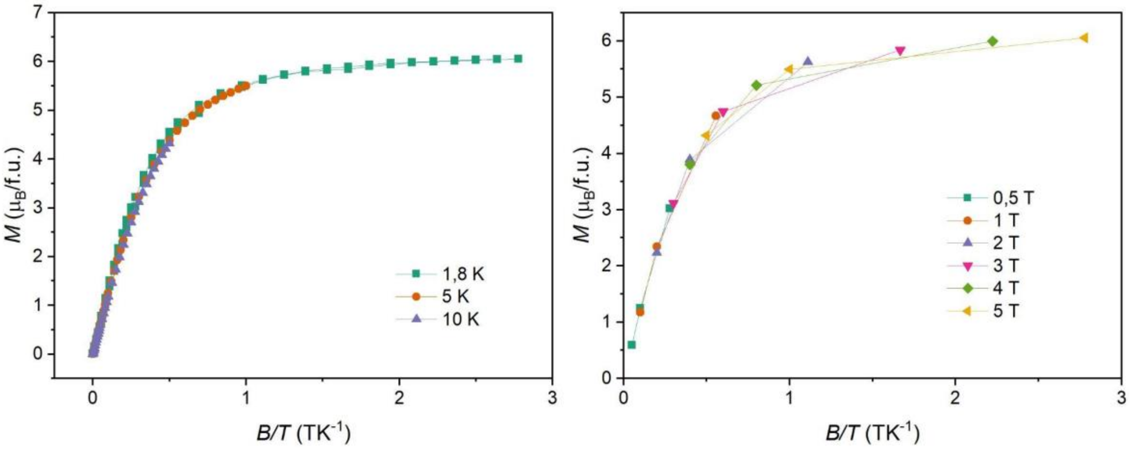

Figure S32. Reduced magnetization plots for [C_2mim][Gd(fod)$_4$] (**4**).

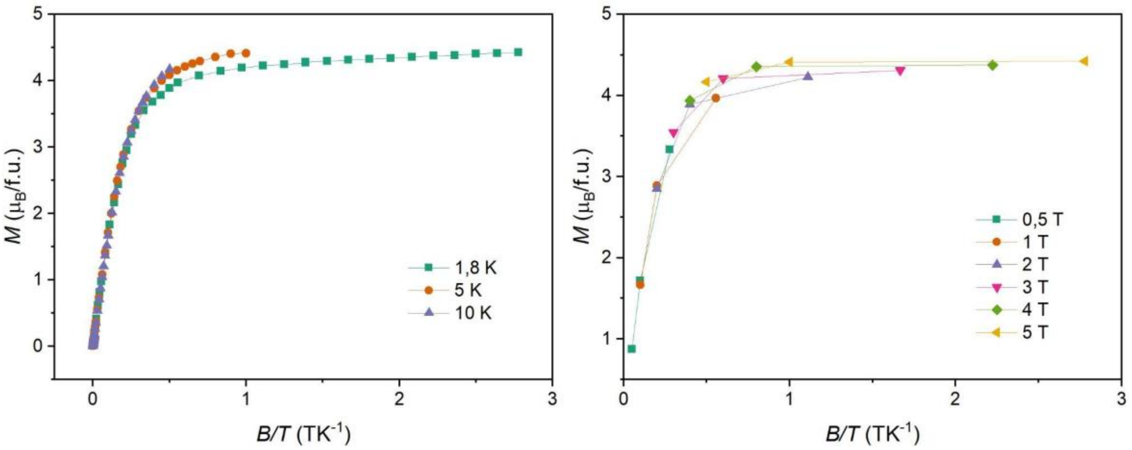

Figure S33. Reduced magnetization plots for [C_2mim][Tb(fod)$_4$] (**5**).

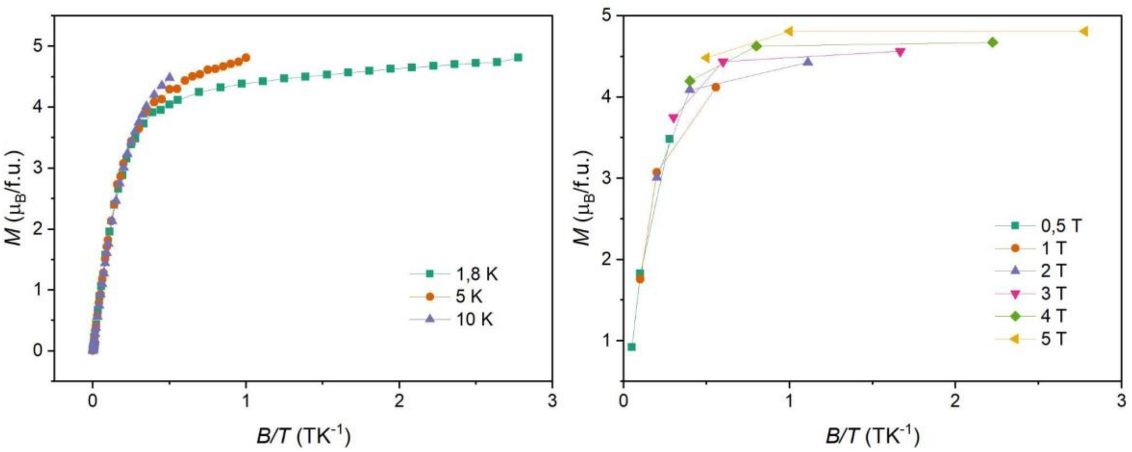

Figure S34. Reduced magnetization plots for [C_2mim][Dy(fod)$_4$] (**6**).

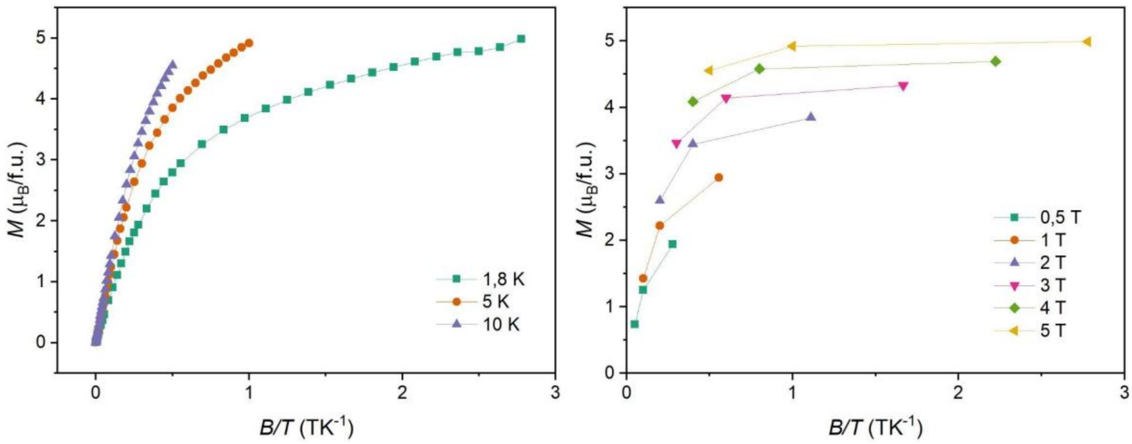

Figure S35. Reduced magnetization plots for [C2mim][Ho(fod)4] (**7**).

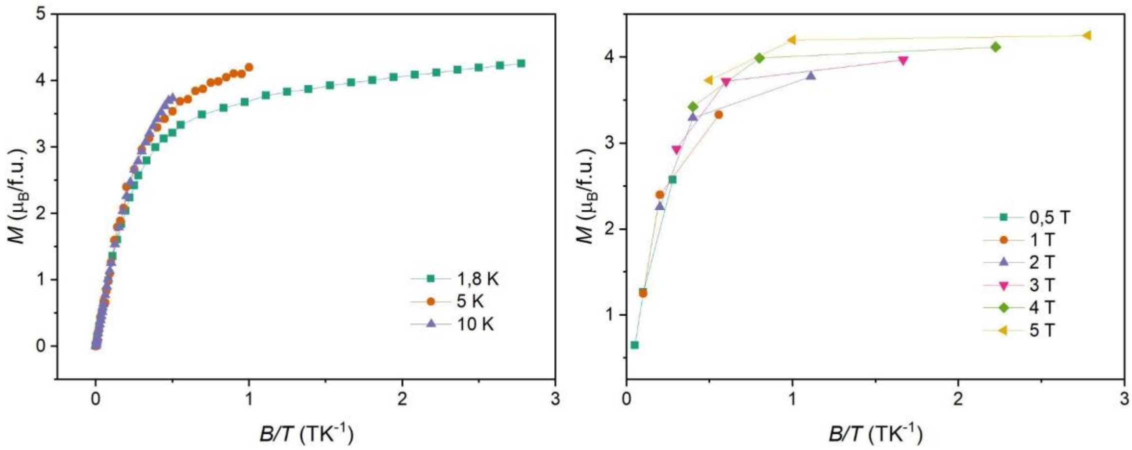

Figure S36. Reduced magnetization plots for [C2mim][Er(fod)4] (**8**).

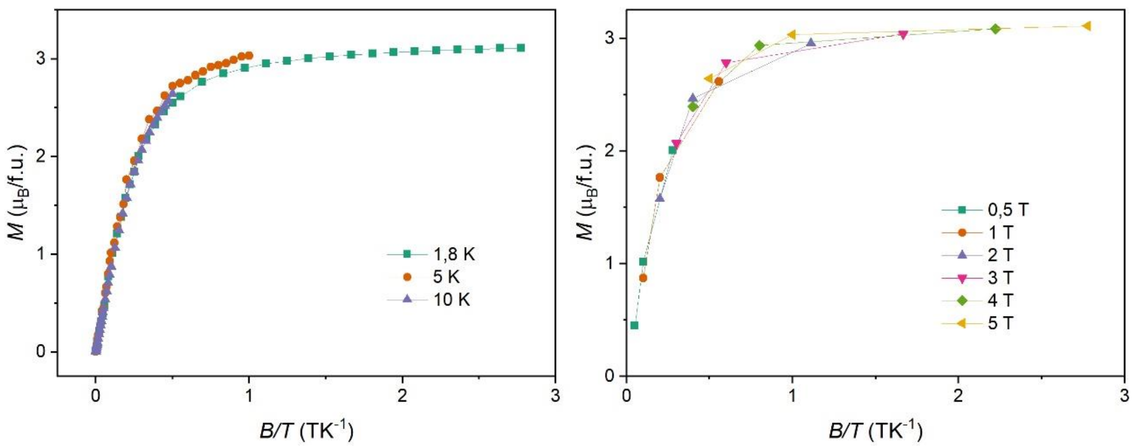

Figure S37. Reduced magnetization plots for [C2mim][Tm(fod)4] (**9**).

7) AC Measurements

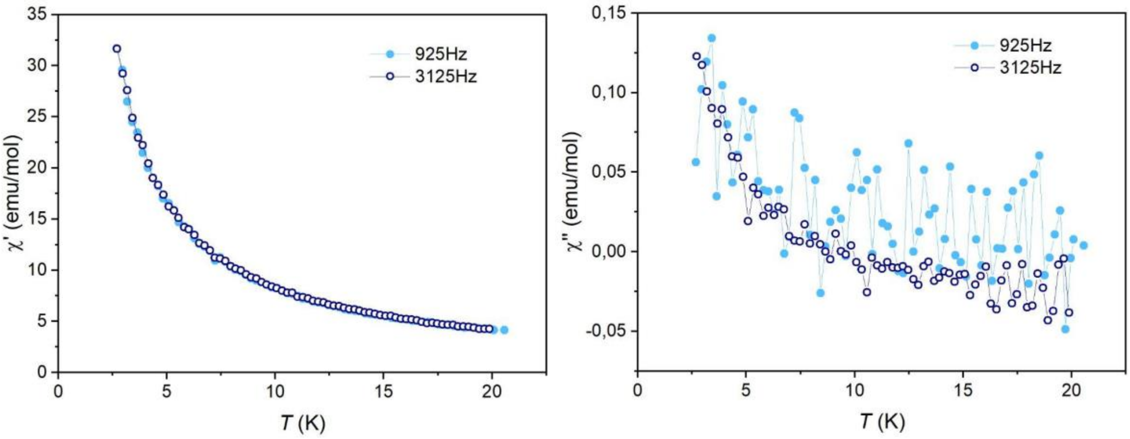

Figure S38. Temperature dependence of the (left) real, χ′, and (right) imaginary, χ′′, components of the AC susceptibility for $[C_2mim][Gd(fod)_4]$ (**4**), collected at different AC frequencies under a static field of H_{DC} = 0 G. H_{AC} = 1 Oe (925 Hz), 3 Oe (3125 Hz).

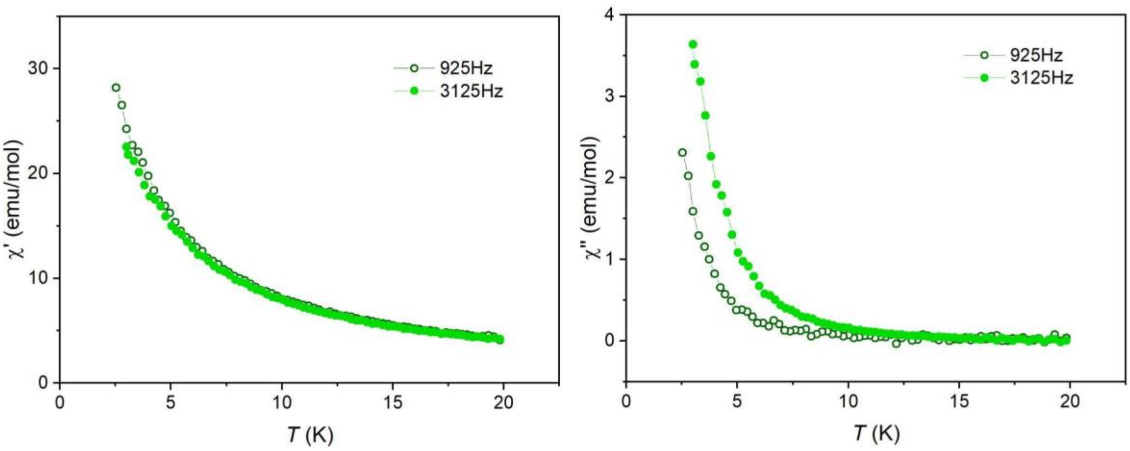

Figure S39. Temperature dependence of the (left) real, χ′, and (right) imaginary, χ′′, components of the AC susceptibility for $[C_2mim][Gd(fod)_4]$ (**4**), collected at different AC frequencies under a static field of H_{DC} = 1500 G. H_{AC} = 1 Oe (925 Hz), 3 Oe (3125 Hz).

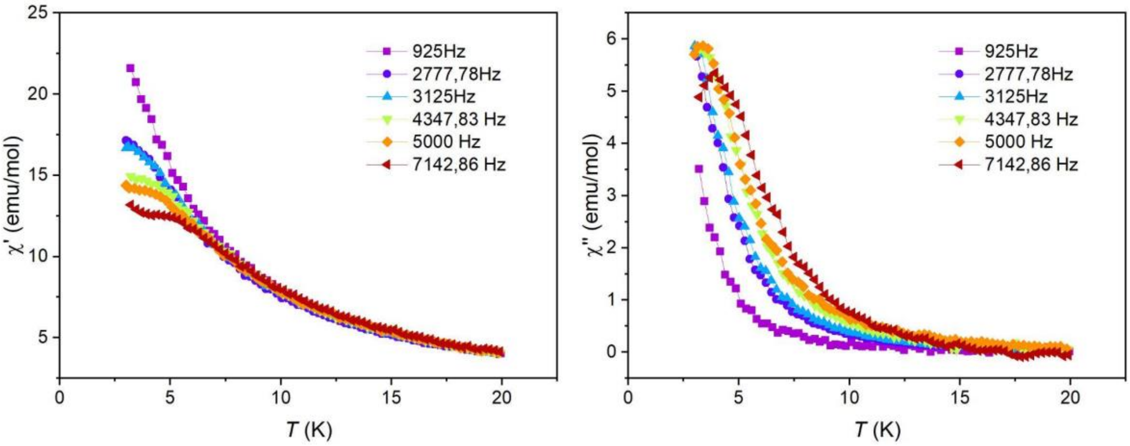

Figure S40. Temperature dependence of the (left) real, χ′, and (right) imaginary, χ′′, components of the AC susceptibility for $[C_2mim][Gd(fod)_4]$ (**4**), collected at different AC frequencies under a static field of H_{DC} = 2500 G. H_{AC} = 1 Oe (925 Hz), 3 Oe (remaining frequencies).

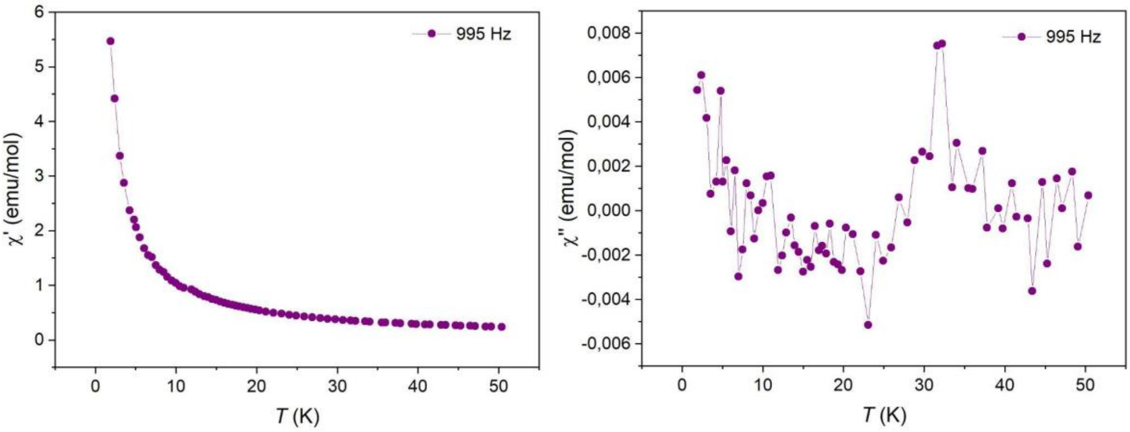

Figure S41. Temperature dependence of the (left) real, χ′, and (right) imaginary, χ′′, components of the AC susceptibility for $[C_2mim][Tb(fod)_4]$ (**5**), collected at AC frequency of 995 Hz under a static field of H_{DC} = 0 G. H_{AC} = 10 Oe.

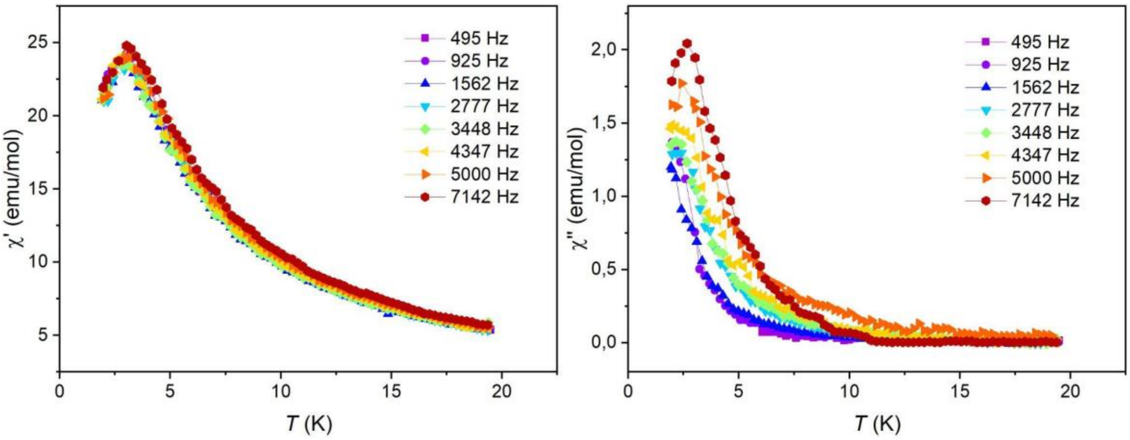

Figure S42. Temperature dependence of the (left) real, χ′, and (right) imaginary, χ′′, components of the AC susceptibility for $[C_2mim][Tb(fod)_4]$ (**5**), collected at different AC frequencies under a static field of H_{DC} = 2500 G. H_{AC} = 3 Oe.

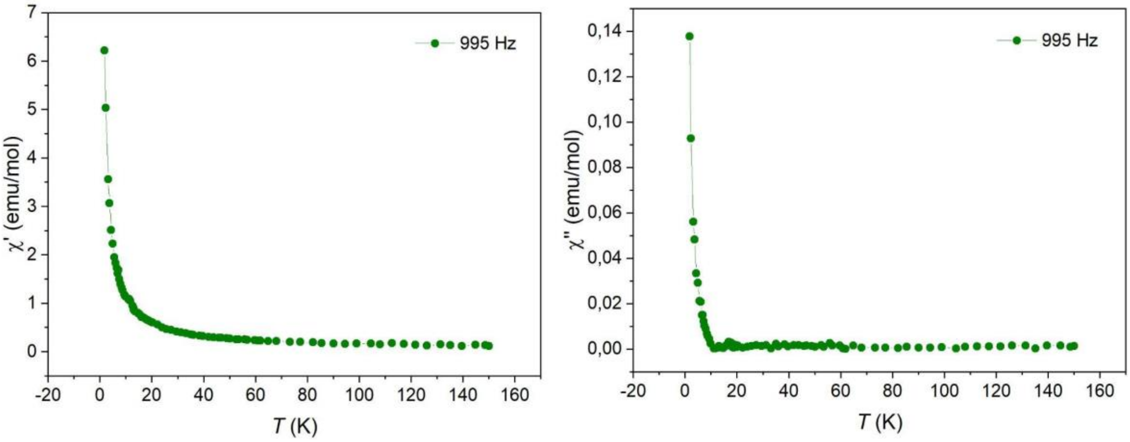

Figure S43. Temperature dependence of the (left) real, χ′, and (right) imaginary, χ′′, components of the AC susceptibility for $[C_2mim][Dy(fod)_4]$ (**6**), collected at AC frequency of 995 Hz under a static field of H_{DC} = 0 G. H_{AC} = 10 Oe.

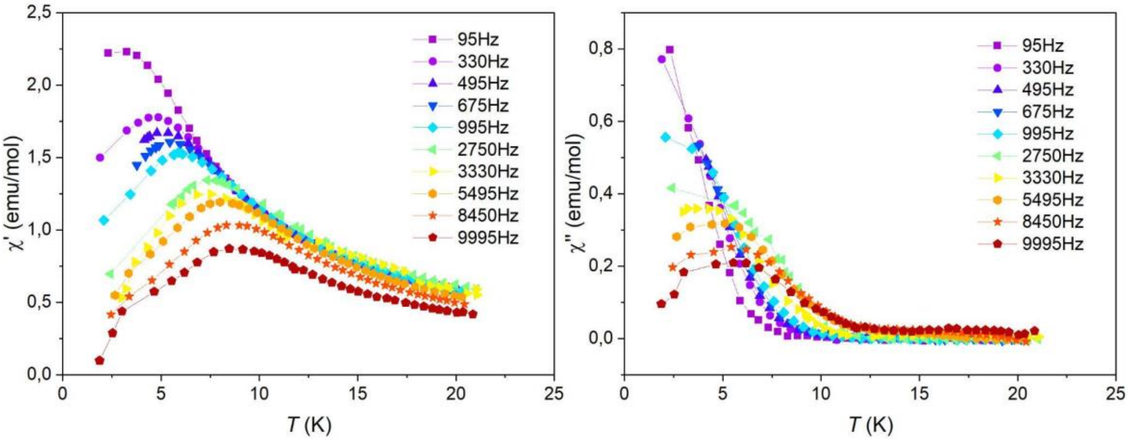

Figure S44. Temperature dependence of the (left) real, χ′, and (right) imaginary, χ′′, components of the AC susceptibility for $[C_2mim][Dy(fod)_4]$ (**6**), collected at several AC frequencies under a static field of H_{DC} = 1500 G. H_{AC} = 10 Oe.

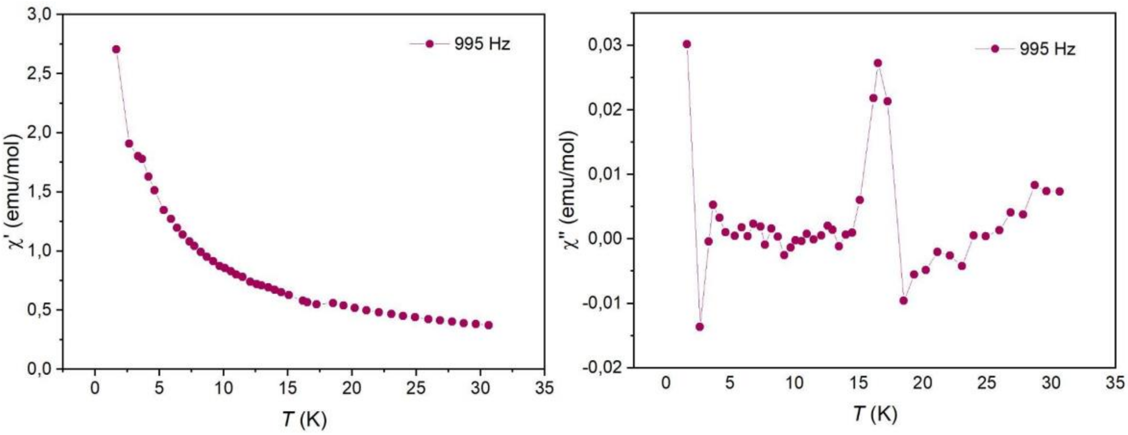

Figure S45. Temperature dependence of the (left) real, χ′, and (right) imaginary, χ′′, components of the AC susceptibility for $[C_2mim][Ho(fod)_4]$ (**7**), collected at AC frequency of 995 Hz under a static field of H_{DC} = 0 G. H_{AC} = 10 Oe.

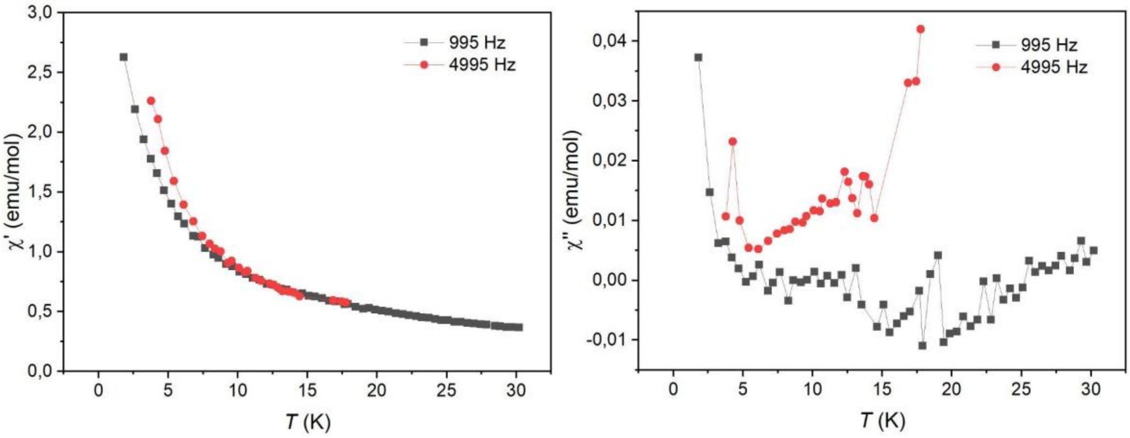

Figure S46. Temperature dependence of the (left) real, χ′, and (right) imaginary, χ′′, components of the AC susceptibility for $[C_2mim][Ho(fod)_4]$ (**7**), collected at different AC frequencies under a static field of H_{DC} = 1000 G. H_{AC} = 10 Oe.

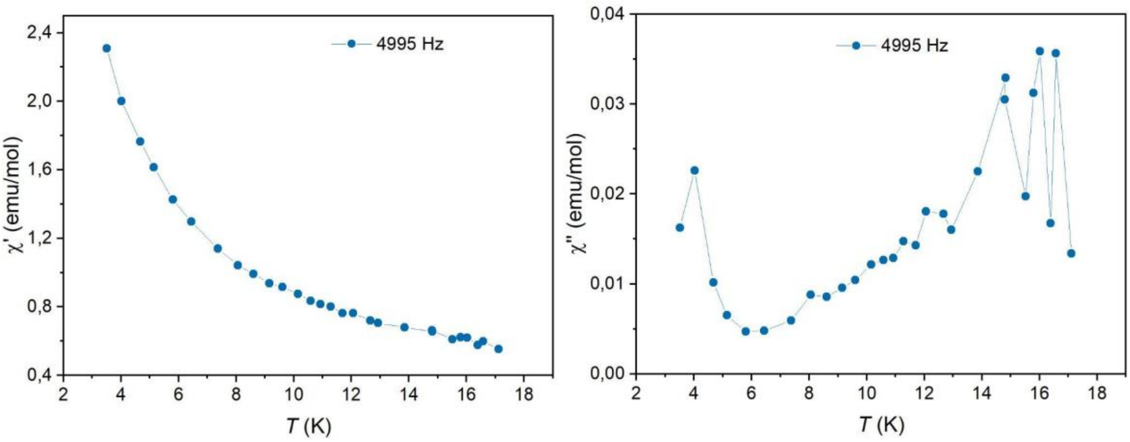

Figure S47. Temperature dependence of the (left) real, χ′, and (right) imaginary, χ′′, components of the AC susceptibility for $[C_2mim][Ho(fod)_4]$ (**7**), collected at AC frequency of 4995 Hz under a static field of H_{DC} = 1500 G. H_{AC} = 10 Oe.

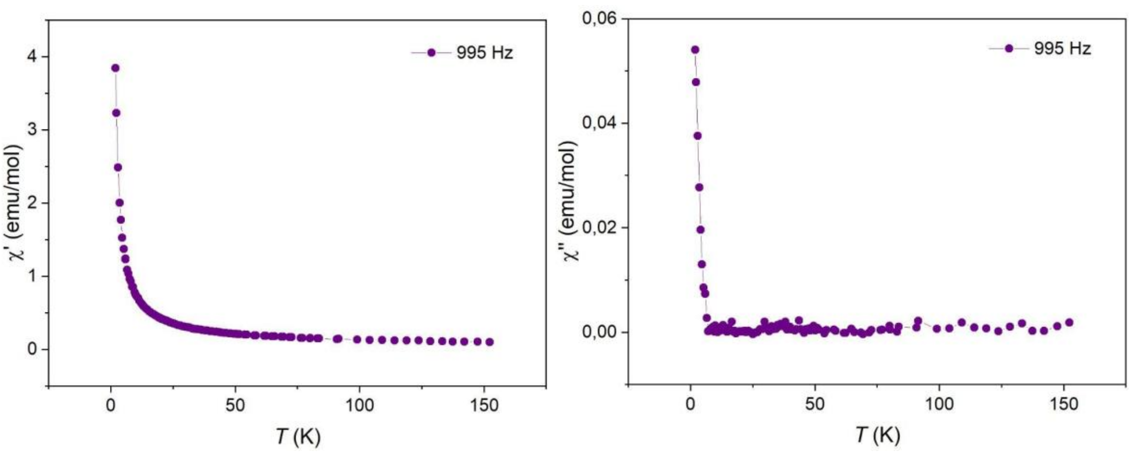

Figure S48. Temperature dependence of the (left) real, χ′, and (right) imaginary, χ′′, components of the AC susceptibility for $[C_2mim][Er(fod)_4]$ (**8**), collected at AC frequency of 995 Hz under a static field of H_{DC} = 0 G. H_{AC} = 10 Oe.

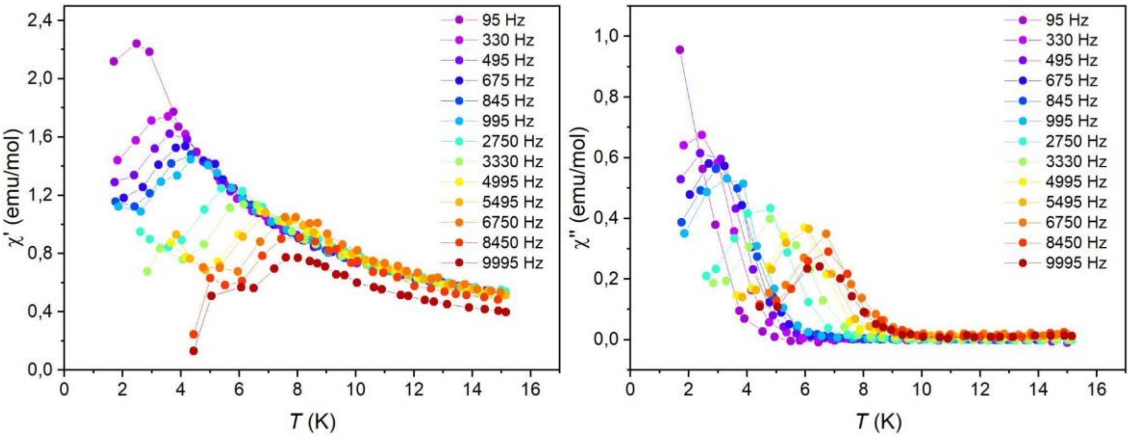

Figure S49. Temperature dependence of the (left) real, χ′, and (right) imaginary, χ′′, components of the AC susceptibility for [C_2mim][Er(fod)$_4$] (**8**), collected at several AC frequencies under a static field of H_{DC} = = 800 G. H_{AC} = 10 Oe.

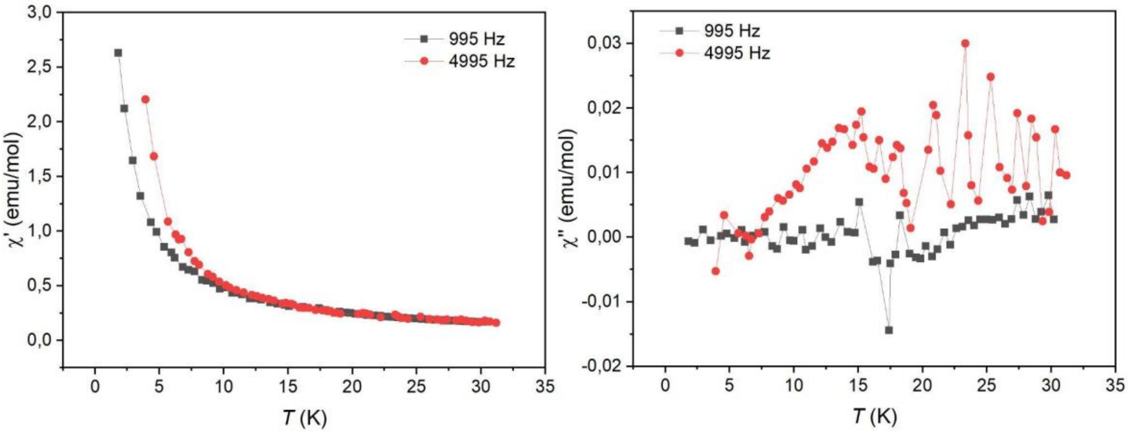

Figure S50. Temperature dependence of the (left) real, χ′, and (right) imaginary, χ′′, components of the AC susceptibility for [C_2mim][Tm(fod)$_4$] (**9**), collected at different AC frequencies under a static field of H_{DC} = 0 G. H_{AC} = 10 Oe.

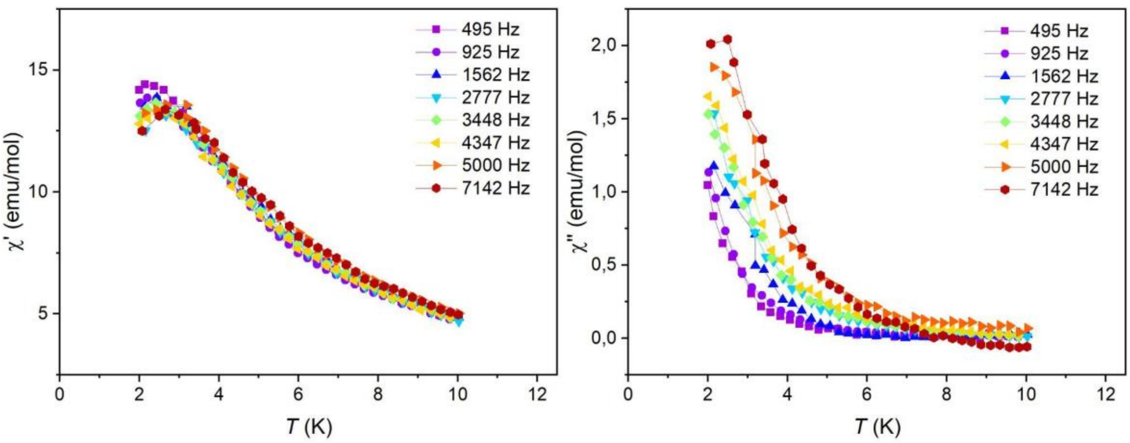

Figure S51. Temperature dependence of the (left) real, χ′, and (right) imaginary, χ′′, components of the AC susceptibility for [C_2mim][Tm(fod)$_4$] (**9**), collected at several AC frequencies under a static field of H_{DC} = 2500 G. H_{AC} = 3 Oe.

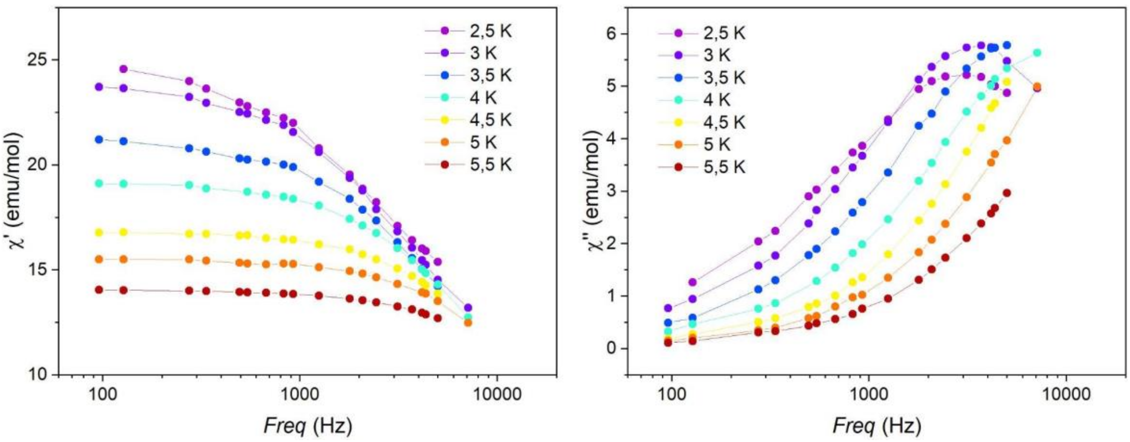

Figure S52. Frequency dependence of the (left) real, χ′, and (right) imaginary, χ′′, components of the AC susceptibility for [C2mim][Gd(fod)4] (**4**), collected at several temperature values under a static field of H_{DC} = 2500 G. H_{AC} = 3 Oe.

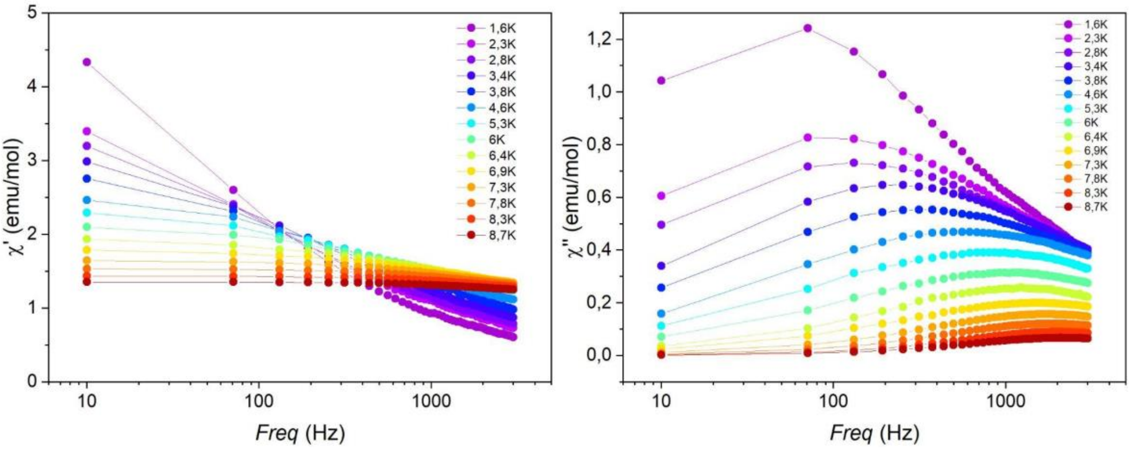

Figure S53. Frequency dependence of the (left) real, χ′, and (right) imaginary, χ′′, components of the AC susceptibility for [C2mim][Dy(fod)4] (**6**), collected at several temperature values under a static field of H_{DC} = 1500 G. H_{AC} = 10 Oe.

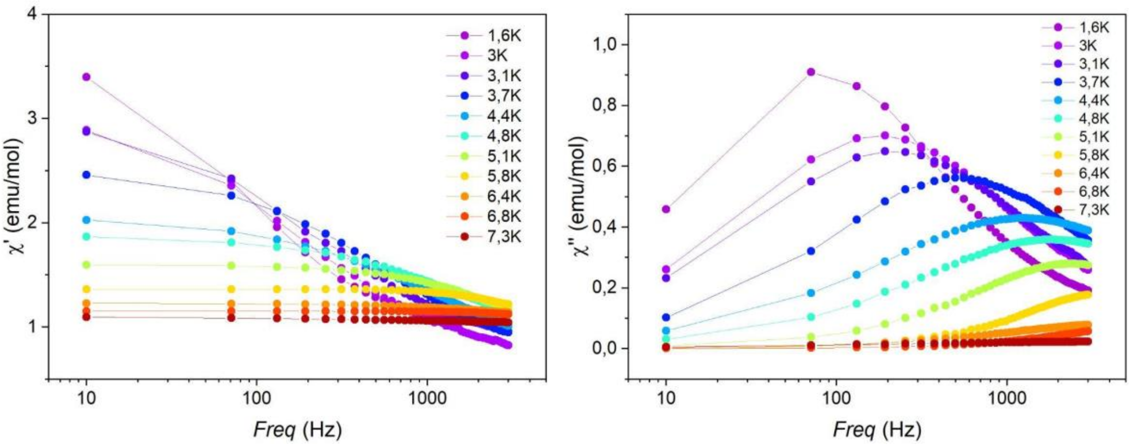

Figure S54. Frequency dependence of the (left) real, χ′, and (right) imaginary, χ′′, components of the AC susceptibility for [C2mim][Er(fod)4] (**8**), collected at several temperature values under a static field of H_{DC} = 800 G. H_{AC} = 10 Oe.

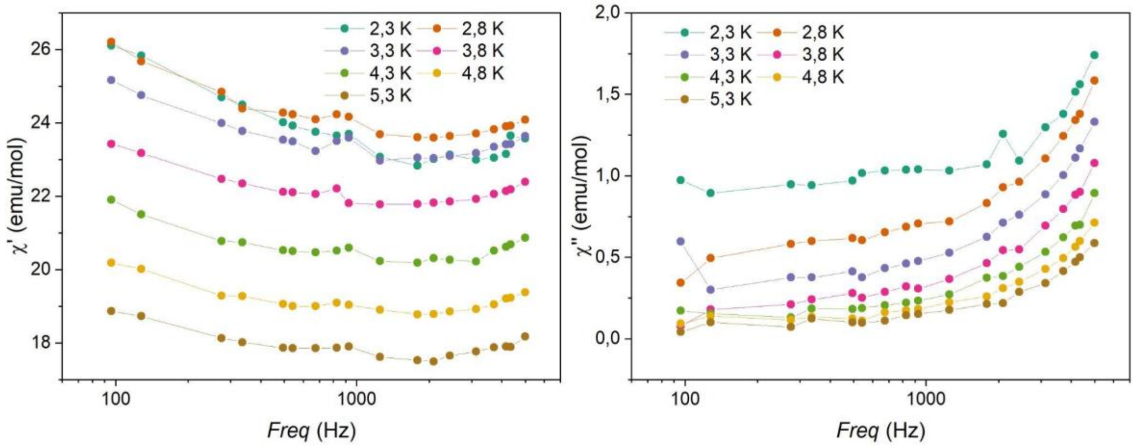

Figure S55. Frequency dependence of the (left) real, χ′, and (right) imaginary, χ′′, components of the AC susceptibility for $[C_2mim][Tb(fod)_4]$ (**5**), collected at several temperature values under a static field of H_{DC} = 1500 G. H_{AC} = 3 Oe.

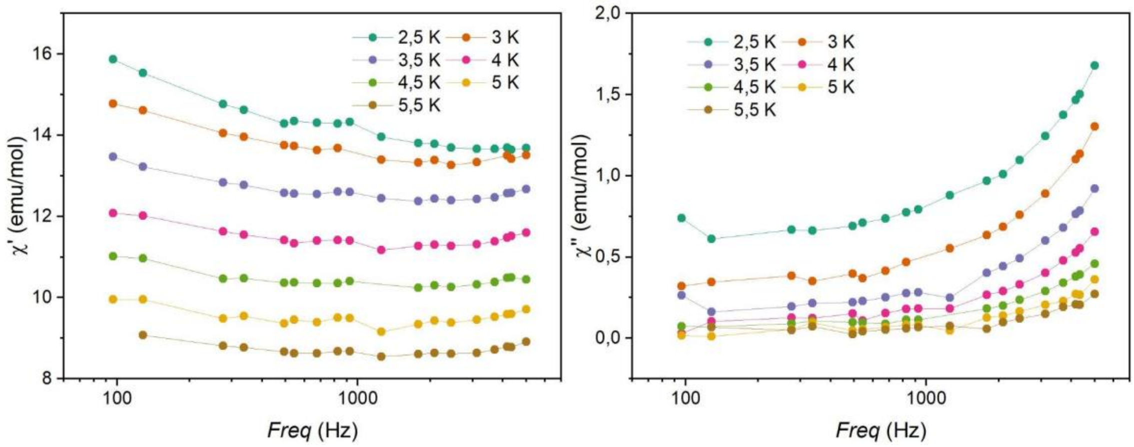

Figure S56. Frequency dependence of the (left) real, χ′, and (right) imaginary, χ′′, components of the AC susceptibility for $[C_2mim][Tm(fod)_4]$ (**9**), collected at several temperature values under a static field of H_{DC} = 2500 G. H_{AC} = 3 Oe.

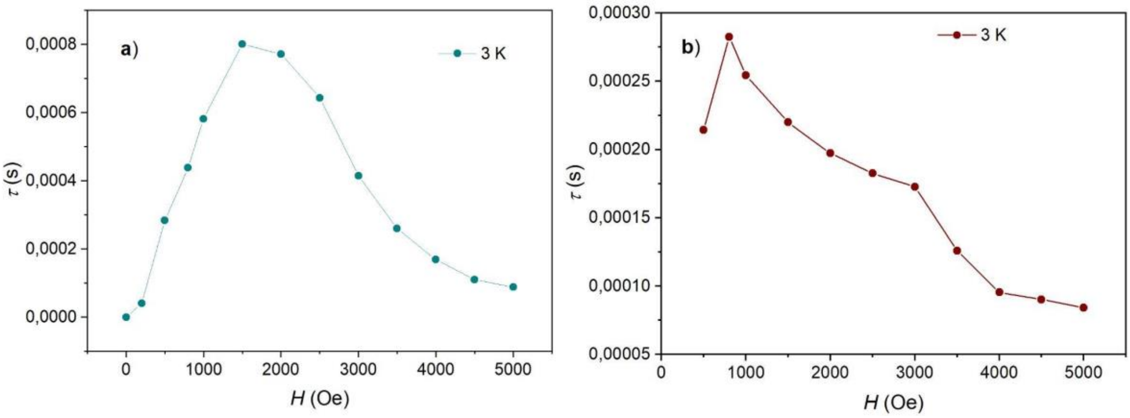

Figure S57. Relaxation times at different static fields for a) $[C_2mim][Dy(fod)_4]$ (**6**), and b) ($[EMIM][Er(fod)_4]$) (**8**), at 3 K and H_{AC} = 10 Oe.

Assuming only an Orbach relaxation process, the obtained values for τ were plotted against the inverse of the temperature and fitted to the Arrhenius law (Eq. S1):

$$\tau(T) = \tau_0 . e^{\left(\frac{U_{eff}}{k_B T}\right)} \qquad \text{(Eq. S1)}$$

where τ_0 is the pre-exponential factor, U_{eff} is the relaxation energy barrier and k_B is the Boltzmann constant. As shown in Figure S47, the fit deviates from linearity at low temperatures being only valid at temperatures higher than 3 K for **4** and **8**, and higher than 2.8 K for **6**, with the following parameters: U_{eff} = 13,06 K with τ_0 = 6,44 x 10^{-7} s (**4**), U_{eff} = 12.19 K with τ_0 = 1,87 x 10^{-5} s (**6**), and U_{eff} = 18.407 K with τ_0 = 1,892 x 10^{-6} s (**8**).

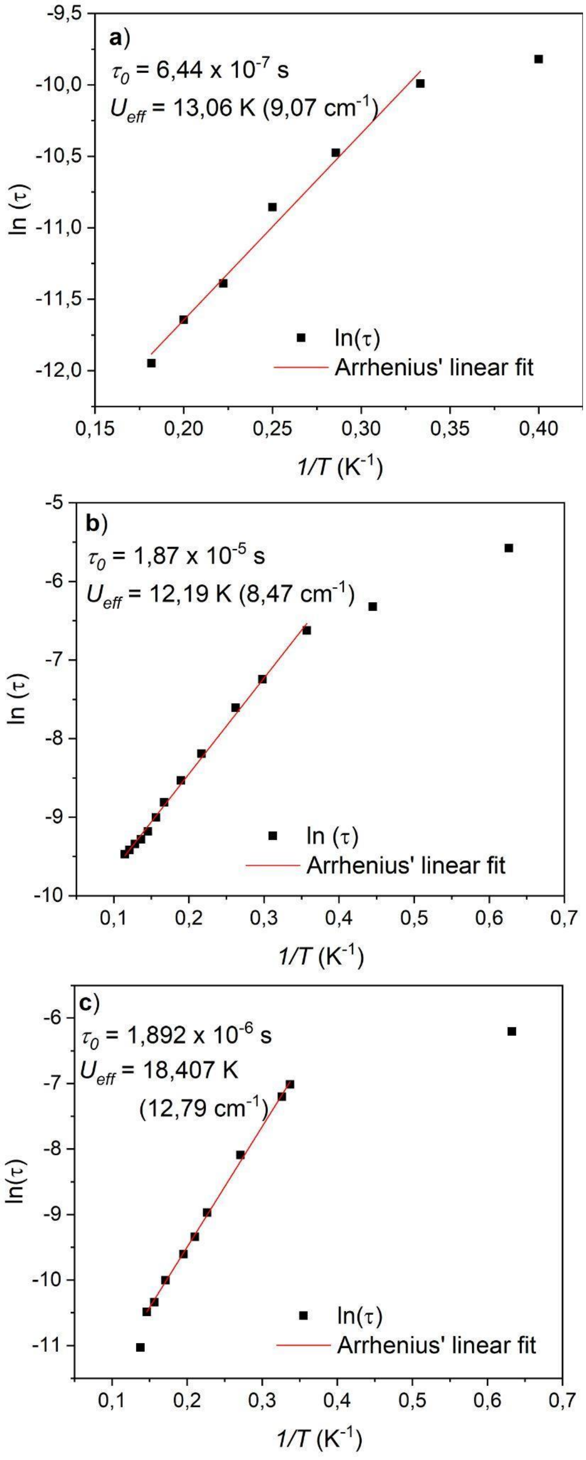

Figure S58. Thermal dependence of the relaxation time τ, measured using an AC field of H_{AC} = 3 Oe, 10 Oe and 10 Oe, and under a static field of H_{DC} = 2500 G, 1500 G and 800 G for (a) **4** ([C_2mim][Gd(fod)$_4$]), (b) **6** ([C_2mim][Dy(fod)$_4$]), and (c) **8** ([C_2mim][Er(fod)$_4$]), respectively. The lines are fits to the Arrhenius equation (eq. S1), assuming an Orbach process.

Table S1. Generalized Debye model fitting parameters under a static field of H_{DC} = 2500 G, in the temperature range of 2.5 to 5.5 K, for [C_2mim][Gd(fod)$_4$] (**4**).

T (K)	α	τ (s)	χ_S (emu.mol^{-1})	χ_T (emu.mol^{-1})
2,5	0,23226	5,4329E-05	9,94754	25,01735
3	0,16657	4,5832E-05	8,87088	23,8067
3,5	0,17098	2,8207E-05	5,9053	21,19856
4	0,15493	1,9290E-05	4,59693	19,18636
4,5	0,11348	1,1311E-05	9,066E-14	16,79233
5	0,10962	8,7811E-06	9,194E-14	15,49594
5,5	0,12945	6,4656E-06	1,635E-14	14,04369

Table S2. Generalized Debye model fitting parameters under a static field of H_{DC} = 1500 G, in the temperature range of 1.6 to 8.7 K, for [C_2mim][Dy(fod)$_4$] (**6**).

T (K)	α	τ (s)	χ_S (emu.mol^{-1})	χ_T (emu.mol^{-1})
1.6	0,47369	0,00379	0,19863	5,98781
2.3	0,51683	0,0018	0,22144	4,35386
2.8	0,51889	0,00133	0,24906	3,94707
3.4	0,48861	0,000715	0,34175	3,40158
3.8	0,50252	0,000497	0,41104	3,0834
4.6	0,48283	0,000277	0,51827	2,67819
5.3	0,48866	0,000197	0,65402	2,44742
6.0	0,46541	0,000149	0,83673	2,19929
6,4	0,39597	0,000123	0,9966	1,9622
6.9	0,35718	0,000103	1,082	1,79996
7.3	0,27099	9,3E-05	1,16229	1,64757
7.8	0,20448	8,77E-05	1,19908	1,53277
8.3	0,13707	8,13E-05	1,2092	1,43096
8.7	0,12093	7,69E-05	1,19148	1,35295

Table S3. Generalized Debye model fitting parameters under a static field of H_{DC} = 800 G, in the temperature range of 1.6 to 7.3 K, for $[C_2mim][Er(fod)_4]$ (**8**).

T (K)	α	τ(s)	χ_S (emu.mol^{-1})	χ_T (emu.mol^{-1})
1.6	0,27687	0,00202	0,91676	3,70575
3.0	0,32286	0,000898	0,65433	3,06394
3.1	0,32952	0,000747	0,75311	3,01623
3.7	0,30377	0,000306	0,65149	2,50921
4.4	0,37103	0,000127	0,48268	2,07115
4.8	0,31804	8,77E-05	0,67234	1,87965
5.1	0,15963	6,74E-05	0,87724	1,59656
5.8	4,38E-17	4,52E-05	1,00445	1,36221
6.4	0,25308	3,24E-05	0,97964	1,22692
6.8	2,37E-15	2,8E-05	1,01228	1,14979
7.3	0,62328	1,62E-05	0,94478	1,10369